diversity

MDPI

Article

Species Diversity and Molecular Characterisation of *Baltoplana* Karling, 1949 (Platyhelminthes, Rhabdocoela, Schizorhynchia): A Taxonomic Revision, Partial Mitogenome Annotation, and Seven New Species †

Jhoe Reyes [1,*], Marlies Monnens [1,2], Laura Vanstraelen [1], Yander L. Diez [3], Philippe E. H. Jouk [1,4], Nathalie J. P. Revis [1], Ernest Schockaert [1], Patrick Reygel [1] and Tom Artois [1]

[1] Centre for Environmental Sciences, Research Group Zoology: Biodiversity and Toxicology, Hasselt University, Agoralaan Gebouw D, B-3590 Diepenbeek, Belgium; marlies.monnens@uhasselt.be (M.M.); laura.vanstraelen@uhasselt.be (L.V.); philippe.jouk@kmda.org (P.E.H.J.); nathalie.revis@uhasselt.be (N.J.P.R.); ernest.schockaert@uhasselt.be (E.S.); patrick.reygel@uhasselt.be (P.R.); tom.artois@uhasselt.be (T.A.)
[2] Royal Belgian Institute of Natural Sciences, OD Taxonomy and Phylogeny, Vautierstraat 29, B-1000 Brussels, Belgium
[3] Smithsonian Marine Station, 701 Seaway Drive, Fort Pierce, FL 34949, USA; yanderluis87@gmail.com
[4] Royal Zoological Society of Antwerp, Centre for Research & Conservation, Koningin Astridplein 20-26, B-2018 Antwerp, Belgium
* Correspondence: jhoe.reyes@uhasselt.be
† This article is registered in ZooBank under: urn:lsid:zoobank.org:pub:97054265-0856-4396-8543-44FA90883E06.

Abstract

We present a taxonomic revision, including phylogenetic analyses of the schizorhynch taxon *Baltoplana* Karling, 1949 (Cheliplanidae). We describe seven new species and provide new morphological data for two known species. Species are mainly distinguished by the morphology and degree of sclerotisation of the male copulatory organ. Three new species are from Australia (*B. bipartita* n. sp., *B. quadricirrata* n. sp., and *B. tricirrata* n. sp.), one from the western Mediterranean (*B. galerita* n. sp.), two from Brazil (*B. pseudovalkanovi* n. sp. and *B. brusai* n. sp.), and one from the USA (*B. floridana* n. sp.). The phylogenetic analysis is based on published and newly obtained 18S and 28S rDNA sequences from six species of the related taxon *Cheliplana* and two of *Baltoplana*, confirming the monophyly of Cheliplanidae. *Baltoplana*, as currently circumscribed, was strongly rejected as monophyletic. The monophyletic status of the genus *Cheliplana* remains uncertain: the species included here form a clade, but with support below the thresholds applied in this study. We also present a partial mitogenome of *B. valkanovi* comprising four protein-coding genes and three tRNAs, and provide an identification key.

Keywords: 18S rDNA; 28S rDNA; Cheliplanidae; Schizorhynchia; phylogeny; meiofauna; microturbellarians; mitogenome

Check for updates

Academic Editor: Greg Rouse

Received: 31 July 2026
Revised: 30 September 2026
Accepted: 7 October 2026
Published: 22 October 2026

Copyright: © 2026 by the authors. Licensee MDPI, Basel, Switzerland. This article is an open access article distributed under the terms and conditions of the Creative Commons Attribution (CC BY) license.

1. Introduction

Marine microturbellarians are mostly free-living platyhelminths that are abundant components of the meiobenthic fauna worldwide [1]. These organisms are generally tiny (<2 mm long) and live mainly among grains of sand and on vegetation, from the intertidal to deep waters [2–4]. These small organisms have been little studied, and many areas of the world remain virtually unsampled; thus, many (new) species remain unrecorded [1]. Among marine microturbellarians, Rhabdocoela Ehrenberg, 1831 is the most species-rich

higher-level taxon, with over 1800 described species [5]. Within it, the monophyletic Kalyptorhynchia Graff, 1905 is defined by a true proboscis, and encompasses the non-monophyletic 'Eukalyptorhynchia' Meixner, 1928 and the monophyletic Schizorhynchia Meixner, 1928 [6,7], the latter characterised by a proboscis that is split into a ventral and a dorsal lip. Schizorhynchia comprises more than 190 marine and brackishwater species and is divided into five families [5]: Cheliplanidae Schilke, 1970, Diascorhynchidae Meixner, 1928, Karkinorhynchidae Meixner, 1928, Nematorhynchidae Schilke, 1969, and 'Schizorhynchidae' Graff, 1905. However, recent molecular studies revealed unresolved relationships within the taxon and indicated that many subtaxa are not monophyletic [6–8].

The family Cheliplanidae contains five genera, all of which have species with a proboscis armed with hooks: *Archipelagoplana* Noldt & Hoxhold, 1984 (1 species), *Baltoplana* Karling, 1949 (4 species), *Cheliplana* de Beauchamp, 1927 (50 species), *Cheliplanilla* Meixner, 1938 (6 species), and *Freddius* Takeda & *Kajihara*, 2018 (1 species) [5]. To date, only three identified species of *Cheliplana* and one species of *Cheliplanilla* have been included in molecular phylogenetic works, providing evidence of the monophyly of Cheliplanidae [7,8]. However, the number of cheliplanids included in phylogenetic analyses is very low considering their diversity, while molecular data are missing for the other three genera within the family.

Mitochondrial genomes constitute a compact but information-rich source of characters for animal systematics because they combine comparatively conserved protein-coding loci with variation in nucleotide composition, RNA features, gene content, and gene order [9–12]. Until recently, mitogenomic data for rhabdocoels included just one free-living and three endosymbiotic species [11]. Initial comparisons revealed significant variations in gene content and arrangement, as well as intrageneric rearrangements and relaxed selective constraints in some protein-coding genes [11]. Monnens et al. [12] expanded the sampling and generated 47 new mitogenomes and showed that rhabdocoel mitogenomes are evolutionarily dynamic. These authors emphasised the need for obtaining more mitogenomes of other free-living lineages to distinguish lineage-specific patterns from those linked to endosymbiosis [12]. Conservative mitogenome annotation is valuable because it enhances taxonomic documentation, enables comparisons with related rhabdocoels, provides reference sequences for future read mapping and assembly, and helps distinguish genuine mitochondrial features from potential artefacts [11,12].

In this contribution, we focus on the taxon *Baltoplana* within Cheliplanidae. This genus was erected by Karling [13] for *B. magna* Karling, 1949 (type species) from the Mediterranean and European Atlantic coasts [13,14]. The four species currently included in *Baltoplana* are: *B. bisphaera* Jouk & De Vocht, 1989 from Kenya, *B. cupressus* Willems & Artois, 2017 from South Africa, *B. magna* distributed in boreal-temperate coastal systems of the North Atlantic (including the Baltic Sea, the North Sea, the French Atlantic coast, the Cantabrian coast, and the northwestern Mediterranean), and *B. valkanovi* Ax, 1959 from the Black Sea [5,13,15–18]. These species share several features with other cheliplanids: they are slender animals without eyes, have a proboscis with hooks, show an adhesive girdle at the posterior end of the body and have a cylindrical, horizontally oriented pharynx with a long prepharyngeal cavity [13,15,16,18]. Species of *Baltoplana* are distinguished primarily by the morphology of their reproductive apparatus [13]. The male system typically includes paired testes and seminal vesicles. The copulatory bulb proper is of the conjuncta-duplex type [19]. It includes a muscular ejaculatory duct, which, distally from the prostate vesicle, forms a cirrus that often is sclerotised. This sclerotisation may be differentiated into ridges or spines, which makes a so-called armed cirrus. This armature appears as spines or ridges within the ejaculatory duct. Apart from the main cirrus, accessory cirri are also present in some species. The female system is characterised by paired ovaries, whereas there is

a single ovary in all other species of Cheliplanidae and in most schizorhynchs (except in *Carcharodorhynchus*). These ovaries are connected to the bursa via sclerotised nozzles and insemination ducts [13,15,16,18].

Here, we present a comprehensive revision of the genus *Baltoplana* that combines morphological and molecular data (18S and 28S rDNA) obtained from six species of *Cheliplana* [*C. cubana* Diez, Gobert, Reygel & Artois, 2021, *C. curacaoensis* Van Steenkiste & Leander, 2021, *C. subproximalis* Diez, Reygel & Artois, 2019, *C. terminalis* Brunet, 1968, *C. boadeni* Schilke, 1970 and *C. remanei* (Meixner, 1928) Karling, 1983] and two species of *Baltoplana* (*B. magna* and *B. galerita* n. sp., see below). In addition, we generate an annotation of the partial mitogenome of *B. valkanovi* Ax, 1959. We provide an overview of the previously known species and describe seven new species collected from different localities worldwide. Finally, we provide an identification key to facilitate the identification of species of *Baltoplana*.

2. Materials and Methods

Morphology: Specimens were extracted from the sediment using the $MgCl_2$ decantation method [20,21]. Animals were studied alive using a compound microscope. Whole mounts were made in lactophenol and later used to study sclerotised structures. When enough specimens were available, some were fixed using Bouin's fixative (50 °C), embedded in paraffin, sagittally sectioned into 4-µm-thick serial sections, and stained using Heidenhain's iron hematoxylin and erythrosine or eosin as counterstain. Whole mounts and sections were studied, photographed, and drawn using a Leica DM2500 LED (Leica Microsystems, GmbH, Wetzlar, Germany) microscope with a camera and a camera lucida, and Differential Interference Contrast. Photographs were made using the Leica Application Suite (LAS X, version 5.3.3, Leica Microsystems) software. Pictures and drawings were processed in Adobe Photoshop CS6® version 13.0 software. Drawings without scale bars are free-hand unless otherwise indicated. Measurements were taken along the central axis of the measured object.

To standardise descriptions of species of *Baltoplana*, we here name the male structures based on Gobert et al. [22], with modifications. We distinguish the following structures:

(a) An ejaculatory duct is a smooth, unarmed, non-sclerotised duct typically surrounded by muscular tissue at its proximal region within the copulatory bulb. The ejaculatory duct may be eversible.

(b) A cirrus refers to a sclerotised portion of the ejaculatory duct that can vary in length and rigidity, the sclerotised region can be located anywhere within the duct. It transports sperm. It may be only slightly sclerotised, resulting in smooth walls within the duct, or heavily sclerotised, leading to the formation of ornamentations, e.g., wrinkles, ridges, and/or spines.

(c) An accessory cirrus (accessory cirri) is a blind sac-like structure within the copulatory bulb that can be everted. It can either be sclerotised, always with ornamentation, such as wrinkles, ridges, and/or spines, or it may not be sclerotised at all. An accessory cirrus is not directly connected to the proximal end of the ejaculatory duct (or cirrus); however, it discharges into the distal end of the ejaculatory duct or cirrus.

(d) A cap is a sclerotised structure that reinforces the (sub)terminal region of the copulatory bulb when the ejaculatory duct or cirrus is extended. When the ejaculatory duct or cirrus is folded back, the terminal region of the cap appears as a "penile/penis papilla" (term used in Gobert et al. [22]), but it should not be regarded as such.

To avoid repetition in the description of species with structures common to *Baltoplana*, *B. tricirrata* n. sp. is described in detail to illustrate the general organisation of the anatomy of the remaining species of *Baltoplana* described herein (see further). Deviating observations

for each (new) species are added in the respective treatments. The species distribution of *Baltoplana* is shown in Figure 1.

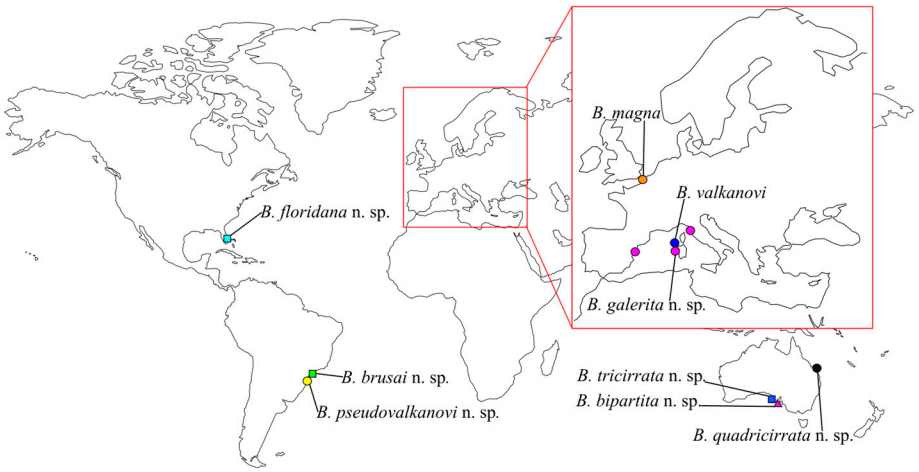


Figure 1. Global distribution of the species of *Baltoplana* treated in this study: the seven new species described here and the two known species for which new material is reported. Only localities represented by specimens examined by us—holotypes, paratypes and additional vouchers—are mapped; records compiled from the literature are not mapped.

For the identification of new species, the phylogenetic species concept (diagnostic version) was applied, which defines species as the smallest diagnosable clusters of individuals that can be distinguished from other such clusters by one or more fixed, diagnostic characters [23]. In practical terms, this means that a group of specimens is recognised as a new species when it consistently differs from another group of specimens by at least one attribute [24]. Species were delimited on morphology. The male copulatory organ provides the fixed, diagnostic characters on which all seven new species are recognised; the female reproductive system, the proboscis apparatus and the habitus are almost invariant across the genus (see Section 4.1). Molecular data were not used to delimit species: sequences were obtained for *B. galerita* n. sp. among the new taxa, and for *B. magna* and *B. valkanovi*, and were generated to test the monophyly of *Baltoplana* and *Cheliplana* within Cheliplanidae. Where available, they corroborate the morphological boundaries. Geographical and habitat data are reported for all species and are consistent with those boundaries, but were not used as delimitation criteria. It should be noted that the authors responsible for the description of the new species are different from the authors of the present article ([25], Art. 50).

DNA extraction, PCR amplification, and sequencing: Specimens for molecular analyses were fixed in 97% ethanol. DNA extraction was performed using a salting-out protocol (adapted from steps 2, 4, and 5 of Laumer [26]). Partial 18S rDNA and 28S rDNA gene fragments were amplified using primers and PCR protocols as described in Table 1.

PCR reactions were conducted using PuReTaq Ready-To-Go PCR beads (GE Healthcare, Little Chalfont, UK). For the amplification of 18S and 28S rDNA, each reaction mixture contained 0.5 µL of each primer (5 µM), 2 µL of DNA extract, and 22 µL of molecular-grade water, resulting in a total volume of 25 µL. The PCR processes were performed using either a Bio-Rad PCR C-1000 or T-100 Touch thermal cycler (Bio-Rad Laboratories, Inc., Hercules, CA, USA), and the resulting products were analysed on a 1.4% agarose gel stained with GelRed™ (Biotium, Inc., Fremont, CA, USA). DNA concentrations were quantified using a Qubit Fluorometer with the Qubit™ dsDNA HS Assay Kit (ThermoFisher Scientific Inc. Waltham, MA, USA). PCR products were purified and sequenced commercially by Macrogen Europe B.V. (Amsterdam, The Netherlands), utilising BigDye™ terminator cycling protocols on an ABI3730XL DNA sequencer (Thermo Fisher Scientific Inc., Foster City, CA, USA).

Phylogenetic molecular analysis: A summary of all sequences used, along with their corresponding accession numbers, is provided in Table 2. Raw reads were quality-trimmed (error probability = 0.05) and assembled in Geneious Prime v2025.0 [27]. Consensus sequences underwent a BLAST version 2.17.0 search [28] on the NCBI website (ncbi.nlm.nih.gov) to identify potential contamination and sequence selection errors. Available sequences of species of Schizorhynchia were retrieved from GenBank [29], and two separate datasets were created for both 18S (48 sequences) and 28S rDNA (41 sequences). We included only sequences with species-level identifications to facilitate a comprehensive analysis of interrelationships and morphological trait evolution. Four species of eukalyptorhynchs served as outgroup: *Cicerina tetradactyla* Giard, 1904, *Paracicerina laboeica* Meixner, 1928 (Cicerinidae), *Polycystis ali* Schockaert, 1982 (Polycystididae), and *Itaipusa divae* Marcus, 1949 (Koinocystididae) as it was used in Diez et al. [8].

Table 1. Primer sequences and PCR regimes used for PCR amplification.

Primer	Direction	Primer Sequence (5′–3′)	Reference
Subunit 18S			
TimA	Forward	AMCTG GTT GAT CCT GCCAG	[30]
TimB	Reverse	TGATCCATCTGCAGGTTCACCT	[30]
Subunit 28S			
LSU5	Forward	TAG GTC GAC CCG CTG AAY TTA	[31]
LSU6-3B	Reverse	GAG AAG GGT TCC ATG TGA ACAGC	[31]

PCR amplification involved treatment at 95 °C for 3 min, 9 × (94 °C for 30 s, 60 °C for 30 s (−0.5 °C/cycle), 72 °C for 90 s), 30 × (94 °C for 30 s, 55 °C for 30 s, 72 °C for 90 s), and 72 °C for 5 min.

Table 2. GenBank accession numbers used in this study for the phylogenetic analyses ("*": new sequences).

Taxa	18S rDNA	28S rDNA
Ingroup		
Cheliplanidae		
B. magna *	PZ724941	–
B. galerita n. sp. F209 *	PZ724942	–
B. galerita n. sp. F212 *	PZ724943	PZ724952
Cheliplana cf. *orthocirra*	AJ012507	-
Cheliplana cubana D22 *	PZ724945	PZ724955
Cheliplana cubana DZ5 *	PZ724946	PZ724956
Cheliplana curacaoensis DC38 *	PZ724947	PZ724957
Cheliplana subproximalis DNA68 *	PZ724949	PZ724959
Cheliplana terminalis DNA9 *	PZ724950	PZ724960
Cheliplana terminalis DNA41 *	PZ724951	PZ724961
Cheliplana terminalis CheTer273OK	OR490852	OR490868
Cheliplana boadeni F249 *	PZ724944	PZ724953
Cheliplana boadeni F321 *	–	PZ724954
Cheliplana remanei F251 *	PZ724948	PZ724958

Table 2. *Cont*.

Taxa	18S rDNA	28S rDNA
Cheliplanilla caudata	KJ887449	KJ887502
"Schizorhynchidae"		
Carcharodorhynchus flavidus	KJ887457	KJ887563
Carcharodorhynchus listensis	OP604377	OP604363
Carolinorhynchus follybeachensis	KR339021	KR339048
Proschizorhynchella quadricaudata	LC512873	LC512874
Proschizorhynchus gullmarensis	OP604375	OP604364
Proschizorhynchus gullmarensis SYLT3	–	KJ887532
Proschizorhynchus tricingulatus	KJ887423	KJ887503
Proschizorhynchus triductibus	AY775744	–
Pseudoschizochilus atlanticus DNA70	PX900315	PX900329
Pseudoschizochilus atlanticus DNA90	PX900316	PX900330
Pseudoschizochilus atlanticus F110	PX900317	PX900331
Pseudoschizochilus atlanticus DJ14	–	PX900327
Pseudoschizochilus atlanticus DJ23	–	PX900328
Pseudoschizochilus lanzarotensis F50	PX900318	PX900332
Pseudoschizochilus lyratus D46	PX900319	PX900333
Pseudoschizochilus lyratus D52	PX900320	PX900334
Pseudoschizochilus lyratus D78	PX900321	PX900335
Pseudoschizochilus lyratus DC12	PX900322	PX900336
Schizochilus caecus	OP604376	OP604365
Schizochilus choriurus	AY775746	–
Schizochilus marcusi	AY775747	–
Schizorhynchoides aculeatus	OP604378	OP604366
Schizorhynchoides canaliculatus	AY775748	–
Schizorhynchoides canaliculatus DNA6SYLIIB	PX900323	PX900337
Schizorhynchoides symetricus MM	PX900326	–
Schizorhynchoides spirostylus F45	PX900325	PX900339
Schizorhynchoides spirostylus F42	PX900324	PX900338
Thylacorhynchus ambronensis	AY775749	–
Thylacorhynchus conglobatus	KJ887448	KJ887534
Diascorhycnhidae		
Diascorhynchus rubrus	AJ012508	AF022752
Diascorhynchus serpens	KJ887439	–
Karkinorhynchidae		
Karkinorhynchus bruneti	AY775740	–
Lehardyia alleithoros	KR339032	JF340473
Outgroup		

Table 2. *Cont*.

Taxa	18S rDNA	28S rDNA
Cicerina tetradactyla	KJ887465	KJ887520
Paracicerina laboeica	KJ887408	KJ887533
Polycystis ali	KJ887460	KJ887523
Itaipusa divae	MW081596	MW054455

Both datasets were aligned in MAFFT v7, as implemented in Geneious Prime version 2026.1.2 [32,33]. The resulting alignments were concatenated in Geneious. The concatenated matrix comprised 53 terminals representing 37 species and 3743 aligned positions (18S, positions 1–1934; 28S, positions 1935–3743), of which 2276 (60.8%) were constant, 1467 (39.2%) variable and 1117 (29.8%) parsimony-informative, distributed over 1777 distinct site patterns. The 18S-only matrix comprised 48 terminals representing 37 species and 1934 positions, of which 1327 (68.6%) were constant, 607 (31.4%) variable and 424 (21.9%) parsimony-informative, over 769 distinct site patterns. Five terminals lacked 18S sequences and twelve lacked 28S sequences, so that 36 of the 53 terminals were represented by both genes; missing entries thus account for 15.8% of the gene-by-terminal cells of the concatenated matrix, while gaps and ambiguities together account for 30.9% of its characters. Substitution models were selected with ModelFinder [34], as implemented in IQ-TREE 3.0.1 [35], under the Bayesian information criterion. For the concatenated matrix, 107 candidate models were compared and GTR+F+R4 was preferred; for the 18S matrix, 74 models were compared and GTR+F+I+R3 was preferred. Because the two markers belong to a single ribosomal cistron, and because the selected free-rate models already accommodate substantial among-site rate variation (four categories spanning an 81-fold range of relative rates in the concatenated matrix), the concatenated alignment was analysed as a single, unpartitioned data block [36]. The consequences of this choice were assessed explicitly (see below).

Maximum-likelihood (ML) analyses were run locally in IQ-TREE 3.0.1 [35,37]: the concatenated matrix under GTR+F+R4 and the 18S matrix under GTR+F+I+R3, in both cases without partitioning. Branch support was evaluated through ultrafast bootstrapping (UFboot) [38] and the Shimodaira–Hasegawa-like approximate likelihood-ratio test (SH-aLRT) [39], executed with 1000 replicates.

To verify that analysing the concatenated matrix without partitioning did not affect the results, it was reanalysed under a two-subset, edge-linked partition model (18S, positions 1–1934; 28S, positions 1935–3743), with substitution models selected independently for each subset (GTR+F+R3 and GTR+F+R4, respectively). The partitioned model fitted the data better (BIC = 59,953.6 versus 60,106.0), but recovered exactly the same topology: the two maximum-likelihood trees share all 50 internal bipartitions (Robinson–Foulds distance = 0). Nodal support was essentially unchanged, with median differences of 0.1 for SH-aLRT and 0 for ultrafast bootstrap across the 50 comparable nodes; only two nodes, both internal to 'Schizorhynchidae' and neither involving *Baltoplana* or *Cheliplana*, crossed the support thresholds defined above. The topology tests described below yielded the same conclusions under both schemes. Since partitioning by gene alters neither the topology nor any of the relationships discussed here, and since rate heterogeneity in ribosomal RNA is governed primarily by secondary structure rather than by gene identity [36], the unpartitioned analyses are reported throughout; the full output of the partitioned analysis is available in Zenodo (see Data Availability Statement).

Bayesian inference (BI) was conducted locally using the Metropolis-coupled Markov Chain Monte Carlo (MC3) algorithm, implemented in MrBayes v3.2.6 [40]. The concate-

nated matrix was divided into two character sets corresponding to the 18S and 28S regions, with substitution parameters and branch lengths linked across them, and analysed under a GTR+Γ model with four rate categories and empirical base frequencies—the closest equivalent available in MrBayes to the free-rate model selected by ModelFinder. Two independent runs, each comprising one cold and three heated chains, were executed concurrently and sampled every 1000 generations, discarding the first 25% of samples as burn-in. The analysis was configured for a maximum of 10,000,000 generations and terminated once the convergence diagnostics had stabilised, following the criterion implemented in the automatic stopping rule of MrBayes. The average standard deviation of split frequencies fell below the conventional threshold of 0.01 after 420,000 generations and remained below it thereafter, plateauing between 0.0043 and 0.0055 over the final 500,000 generations; the runs were accordingly stopped at 1,914,000 generations, with a final value of 0.0047, a potential scale reduction factor of 1.00 for all estimated parameters, minimum effective sample sizes above 1100, and log probabilities at stationarity in both runs. The resulting topologies were summarised in an extended majority-rule (allcompat) consensus tree. Inferred posterior probabilities (pp) were used as support values. The ML and BI trees were visualised and rooted using FigTree v1.4.4 [41]. Branches with low support values SH-aLRT < 80, UFboot < 90, or pp < 0.95 were collapsed.

Testing the monophyly of Baltoplana and *Cheliplana*: The monophyly of *Baltoplana* and *Cheliplana* was evaluated using likelihood-based topology tests implemented in IQ-TREE 3. Two molecular datasets were analysed independently: (1) a concatenated dataset comprising partial 18S and 28S rRNA gene sequences and (2) a dataset comprising only 18S rRNA sequences. For each dataset, an unconstrained maximum-likelihood (ML) tree was inferred under the model selected for that dataset by ModelFinder (GTR+F+R4 for the concatenated matrix, GTR+F+I+R3 for the 18S matrix). Separate constrained ML searches were subsequently performed for each genus by enforcing the monophyly of the corresponding taxa using a constraint tree. For *Baltoplana*, the constrained hypothesis specified a monophyletic group comprising *B. magna* and the two specimens of *B. galerita* n. sp. For *Cheliplana*, the constrained hypothesis specified a monophyletic group comprising all species assigned to *Cheliplana* in the corresponding alignment. For each genus and dataset, the unconstrained and corresponding constrained trees were combined into a single candidate-tree file and evaluated against the corresponding molecular alignment. Their fit to the data was compared using the Kishino–Hasegawa test (KH; [42]), Shimodaira–Hasegawa test (SH; [43]), and Approximately Unbiased test (AU; [44]). All topology tests were conducted using 10,000 resamplings based on the RELL approximation. Within each test, site-wise log-likelihoods for the competing topologies were computed on the same alignment and under the same substitution model, so that candidate trees differed only in topology. The exact command lines are provided in the Supplementary Material. Differences between competing topologies were considered statistically significant when $p < 0.05$. Rejection of the constrained topology was interpreted as evidence that the current circumscription of the corresponding genus is incompatible with the topology recovered from the sample taxa in that molecular dataset, and not as a demonstration that the genus is polyphyletic.

(1) Concatenated 18S–28S analysis: The concatenated analysis included all available partial 18S and 28S rRNA sequences. Because 28S sequences were unavailable for *B. magna* and *B. galerita* n. sp. F209, the corresponding positions were coded as missing data in the concatenated alignment. An unconstrained ML tree was inferred and compared with a constrained topology enforcing the monophyly of the clade consisting of *B. magna* and *B. galerita* n. sp. (isolates F209 and F212). For *Cheliplana*, the unconstrained ML tree was compared with a constrained topology enforcing the monophyly of the clade consisting of all seven species of *Cheliplana* (and their isolates) represented in the concatenated alignment.

The genus-specific candidate topologies were evaluated using the KH, SH, and AU tests described above.

(2) 18S analysis: To assess whether the absence of 28S data for some specimens of *Baltoplana* influenced the topology-test results, a second analysis was conducted using only 18S rRNA sequences, the marker available for all three specimens of *Baltoplana*. An unconstrained ML tree was inferred from the 18S alignment and compared with a topology enforcing the monophyly of the clade consisting of *B. magna* and *B. galerita* n. sp. The 18S alignment contained 10 isolates of *Cheliplana*, accounting for seven species; *C. boadeni* (isolate F321) was not represented in this matrix. The unconstrained 18S tree was, therefore, also compared with a constrained topology enforcing the monophyly of *Cheliplana* (10 isolates) included in the alignment. The genus-specific candidate topologies were evaluated using the KH, SH, and AU tests with 10,000 RELL resamplings, following the same significance criterion applied to the concatenated dataset.

Sequencing, assembly and annotation of the partial mitogenome: Total genomic DNA of *B. valkanovi* was extracted using the salting-out protocol described above. The quantity of double-stranded DNA was quantified using a Qubit® 2.0 Fluorometer (Life Technologies, Paisley, UK). An aliquot of 30 µL DNA at a concentration of 10 ng/µL was sent to Macrogen Europe (Amsterdam, The Netherlands) for DNA purification, followed by sample quality assessment using TapeStation analysis. Sequencing libraries were prepared using the Watchmaker PCR-based DNA Library Preparation Kit, and library quality was assessed by qPCR and TapeStation analysis prior to sequencing on an Illumina NovaSeq X platform in paired-end mode (2 × 151 bp). Approximately 2 GB of sequence data were generated for the sample. The resulting demultiplexed reads were submitted to the NCBI Sequence Read Archive (ncbi.nlm.nih.gov/sra) under BioProject accession number PRJNA1533030.

The mitochondrial assembly strategy followed the targeted seed-and-extend approach used by Monnens et al. [11], with modifications to accommodate an incomplete, repeat-rich assembly. NOVOPlasty v4.3.5 [45] was run in mitochondrial mode on 22,365,194 paired reads, using a k-mer size of 25, an expected genome-size range of 12,000–22,000 bp and a nominal insert size of 300 bp with automatic insert-size estimation. A 658-bp partial *cox1* sequence from the closely related rhabdocoel *Cheliplana setosa* (GenBank MG256123) was used solely to recruit mitochondrial reads and was not used as a scaffold or annotation reference. NOVOPlasty produced two alternative assemblies. Although both outputs were labelled circular by Geneious Prime version 2026.1.2, neither contained independent evidence sufficient to establish a complete circular mitochondrial genome. Assembly option 1 contained the validated protein-coding and RNA loci and was retained as the principal partial mitochondrial sequence. Raw-read quality was assessed using FastQC v0.12.1 [46] in Geneious Prime. Adapter and quality trimming were then performed in Geneious Prime with BBDuk v38.84. Low-quality bases were trimmed from both ends at Q20; paired-read overhang trimming used a minimum overlap of 20 bp; and reads shorter than 50 bp after trimming were discarded.

Initial feature prediction was performed with MITOS2 through the Galaxy Europe Server by uploading paired-end fastq reads for bioinformatic analysis [47]. Annotations were imported into Geneious Prime version 2026.1.2 [27,48,49]. MITOS2 calls were treated as provisional hypotheses rather than accepted annotations. All protein translations used the NCBI translation Table 9 (Echinoderm and Flatworm Mitochondrial Code).

Comparative annotation was guided by a curated reference collection derived from the rhabdocoel mitochondrial sequences analysed by Monnens et al. [12] (Table 3). Each candidate protein-coding gene was evaluated by using MUSCLE v5.1 [50] in Geneious Prime. The candidate was compared with homologous rhabdocoel mitochondrial sequences, translated under genetic code 9 and inspected for reading-frame continuity, plausible start

and stop codons, expected gene length and the absence of internal stop codons. BLAST similarity searches [51] were used when needed to confirm gene identity, and features were retained only when all criteria were satisfied.

Table 3. Rhabdocoel mitochondrial sequences used for comparative annotation of the partial mitogenome of *Baltoplana valkanovi*.

Species	GenBank Accession Number(s)	Reference
Anoplodiopsis gracilis	PV804650, PV804651, PV804652, PV804654, PV804678	[12]
Anoplodium hymanae	PV804674	[12]
Anoplodium stichopi	PV804689	[12]
Anoplodium tubiferum	PV804679, PV804680, PV804682, PV804683, PV804715	[12]
Baicalellia brevituba	PV804694	[12]
Baicalellia daftpunka	PV804687, PV804688	[12]
Bothromesostoma personatum	MF993329	[11,12,52]
Graffilla buccinicola	MT063059	[11]
Orostylis caecus	PV804698, PV804699	[12]
Paravortex cf. *cardii*	PV804664, PV804665, PV804666, PV804716	[12]
Pogaina paranygulgus	PV804705, PV804706, PV804707	[12]
Pogaina sp. 'Cuba'	PV804695, PV804696, PV804697	[12]
Provortex balticus	PV804646, PV804653	[12]
Provortex karlingi	PV804681	[12]
Provortex nov. sp. WIM	PV804663	[12]
Provortex psammophilus	PV804662	[12]
Pterastericola astropectinis	PV804655, PV804656, PV804657, PV804658, PV804659, PV804660, PV804669, PV804670, PV804671, PV804702, PV804703, PV804704, PV804708, PV804709, PV804710, PV804711, PV804712, PV804713, PV804714, PV804717, PV804718	[12]
Pterastericola pellucida	PV804640, PV804641, PV804642, PV804643, PV804644	[12]
Syndesmis aethopharynx	PV804684, PV804686	[12]
Syndesmis aff. *albida* 'Evy'	PV804667, PV804701	[12]
Syndesmis albida	PV804648	[12]
Syndesmis albida 'zwartstip'	PV804645	[12]
Syndesmis cf. *aethopharynx*	PV804673, PV804675	[12]
Syndesmis echinorum	MT063058	[11]
Syndesmis kurakaikina	MT063057	[11]
Syndesmis rubida	PV804647, PV804649, PV804668, PV804672	[12]
Syndesmis sp. SAR	PV804685	[12]
Tamanawas kalipis	PV804690, PV804691, PV804692, PV804693	[12]
Umagilla forskalensis	PV804676, PV804677, PV804700	[12]
Vejdovskya ignava	PV804661	[12]

The entire 7154-bp assembled contig was submitted to tRNAscan-SE v2.0 in Organellar mode. This analysis used the Infernal first-pass search at maximum sensitivity, along with the echinoderm/flatworm mitochondrial genetic code [53,54]. The results included predictions of isotype, anticodon, coordinates, score, and secondary structure representations (generated by NAVIEW). For each candidate tRNA, the extracted sequence and homologous, previously annotated rhabdocoel tRNAs were aligned with the MAFFT v7.511 web server using Q-INS-i, which incorporates RNA secondary-structure information [32,55]. Alignments were inspected for placement of the proposed anticodon in the homologous anticodon block, conservation of adjacent positions, internal gaps, terminal alignment and consistency of candidate boundaries with the reference set. Taxonomically incoherent references were removed only when they degraded the homologous structural alignment; the reduced reference set and rationale were recorded in the validation log. A tRNA was accepted only when independent evidence was convergent: a compatible MiTFi prediction, homologous Q-INS-i alignment, a plausible anticodon and cloverleaf-like secondary structure, and—where repeats made placement ambiguous—read support from unique flanks. In addition, assembly joins and duplicated features were assessed from reads that crossed candidate boundaries into a unique flanking sequence, considering read direction, pair consistency, and alignment identity. The absence from tRNAscan-SE was not, by itself, considered evidence of absence, because divergent flatworm mitochondrial tRNAs may be difficult to detect with general organellar models. Because the assembly remained partial, failure to annotate additional rRNA, tRNA or protein-coding loci was treated as non-recovery rather than evidence of biological absence. Such loci may lie outside the recovered fragment, and highly divergent flatworm mitochondrial genes, structurally reduced tRNAs and uncertain rRNA boundaries may be missed or remain insufficiently supported by automated annotation alone [10–12,48]. The mitochondrial genome map was created using the OrganellarGenomeDRAW (OGDRAW) version 1.3.1 server [56], and the 2D tRNA models were edited using Adobe Photoshop CS6® version 13.0 software.

Reads were remapped against the assembled contig in Geneious Prime v2026.1.2 [27] using the built-in Geneious mapper (Medium Sensitivity/Fast, fine tuning iterated up to five times, gaps allowed to a maximum of 15% per read and 50 bp, maximum 30% mismatches per read, maximum ambiguity 4). Because alignment settings were deliberately permissive, so that divergent or junction-spanning reads would not be excluded at the alignment stage, reads whose placement was ambiguous—that is, for which the mapper reported an alternative position of comparable score—were set aside when inspecting candidate boundaries. This screen was used to guide inspection only; no annotation reported here rests on it. Support for the continuity of the assembly across the linearisation point was assessed independently of read mapping: the 50-bp sequence spanning positions 7130–7154 and 1–25 was searched for as an exact match in the raw read pool. Of 22,365,194 reads, 829 contained the complete junction sequence, representing 81% of all reads carrying the 25-bp upstream flank; the remainder are accounted for by reads in which the flank falls at the read end. These reads support the local continuity of *cox1* across the boundary, but do not establish circularity of the mitochondrial chromosome.

Type material and storage: The holotypes of the species described from Australian material are deposited in Australian collections: Australian Helminthological Collection (AHC), South Australian Museum, and The Australian Museum (W). Specimens collected in the United States are deposited in the National Museum of Natural History (USNM), Smithsonian Institution. The remaining holotypes are deposited in the collection of the Finnish Museum of Natural History (KT), Helsinki, Finland. Paratypes and reference material are deposited in the collection of the Research Group 'Zoology: Biodiversity and Toxicol-

ogy', Hasselt University, Belgium (HU). The authors contributed differently to the species descriptions, reflected in the different authorships of the new species.

3. Abbreviations to the Figures

ac: Accessory cirrus; ag: adhesive girdle; b: bursa; bn: bursal nozzle; bs: bursa stalk; bg: bursal gland; ca: sclerotic cap; cb: copulatory bulb; cga: common genital atrium; ci: cirrus; ed: ejaculatory duct; gp: gonopore; h: hook; hs: hook support; i: intestine; ic: insemination duct; od: oviduct; ov: ovary; m: mouth; p: proboscis; pg: prostatic gland; ph: pharynx; ppc: pre-pharyngeal cavity; sp: spine; sr: sclerotised ring; tf: tactile finger; t: testis; vit: vitellarium; sv: seminal vesicle.

4. Results

4.1. Taxonomical Account

Kalyptorhynchia Graff, 1905
Schizorhynchia Meixner, 1928
Cheliplanidae Schilke, 1970
Baltoplana Karling, 1949
Baltoplana tricirrata n. sp. Reyes, Jouk & Artois
urn:lsid:zoobank.org:act:6AFBDA2E-DE8B-4BDF-839D-2D66EC066553
Figure 2

Type material: *Holotype*: Australia • One whole mount; Port Lincoln, Coffin Bay National Park, beneath Golden Island Lookout, coarse-grained sand, ca. 20 cm deep; −34.687778, 135.327139 (type locality); 8 December 2010; AHC37225. *Paratype*: Australia • One whole mount; Port Lincoln, Coffin Bay National Park, beneath Golden Island Lookout, small bay with coarse-grained sand and shell gravel; −34.687944, 135.327806; 8 December 2010; HU IV.4.31. • Three histological sections; one with the same data as for the holotype; HU IV.4.32; two with the same data as for the paratype; HU IV.4.34, HU IV.4.33.

Etymology: The species name refers to the number of accessory cirri of the male copulatory organ (Latin: *tri*, derived from *tres* = three, and *cirratus*, an adjective derived from *cirrus*).

Diagnosis: Species of *Baltoplana* with a ~208-µm-long spiny cirrus and three spiny accessory cirri. One of the accessory cirri is elongated, ~83 µm long, while the other two are spherical or oval, ~44 µm and ~28 µm long, respectively.

Description: The whole-mounted animals are 0.9–2.6 mm long ($\bar{x}$ = 1.6 mm, n = 3). A haptic girdle is present just anterior to the posterior end of the body (Figure 2A), while the posterior end itself contains haptic glands (Figure 2E). The proboscis is 90–131 µm long ($\bar{x}$ = 107 µm, n = 3) (Figure 2(A,B1,B2)). The epidermis is syncytial, 5–7 µm thick and is covered with 9–15-µm-long cilia. Small, ovoid epidermal rhabdites are sparsely scattered across the entire body surface (Figure 2E). The proboscis hooks are 41–46 µm long ($\bar{x}$ = 44 µm, n = 6), slender, curved, and without denticles (Figure 2(B1,B2)). The muscular hook supports are 51–72 µm long ($\bar{x}$ = 61 µm, n = 6). Soft tactile fingers are between the two muscular hook supports (Figure 2(B1,B2)). The brain is situated behind the proboscis. The mouth is located ventrally, posterior to the proboscis bulb. The mouth connects to a long prepharyngeal cavity, which leads to an elongated, cylindrical pharynx positioned in the anterior third of the body (Figure 2A). This prepharyngeal cavity is covered by small, sclerotised spines and is lined by inner longitudinal and outer circular muscle layers. Glandular cells open at the posterior region of the pharynx.

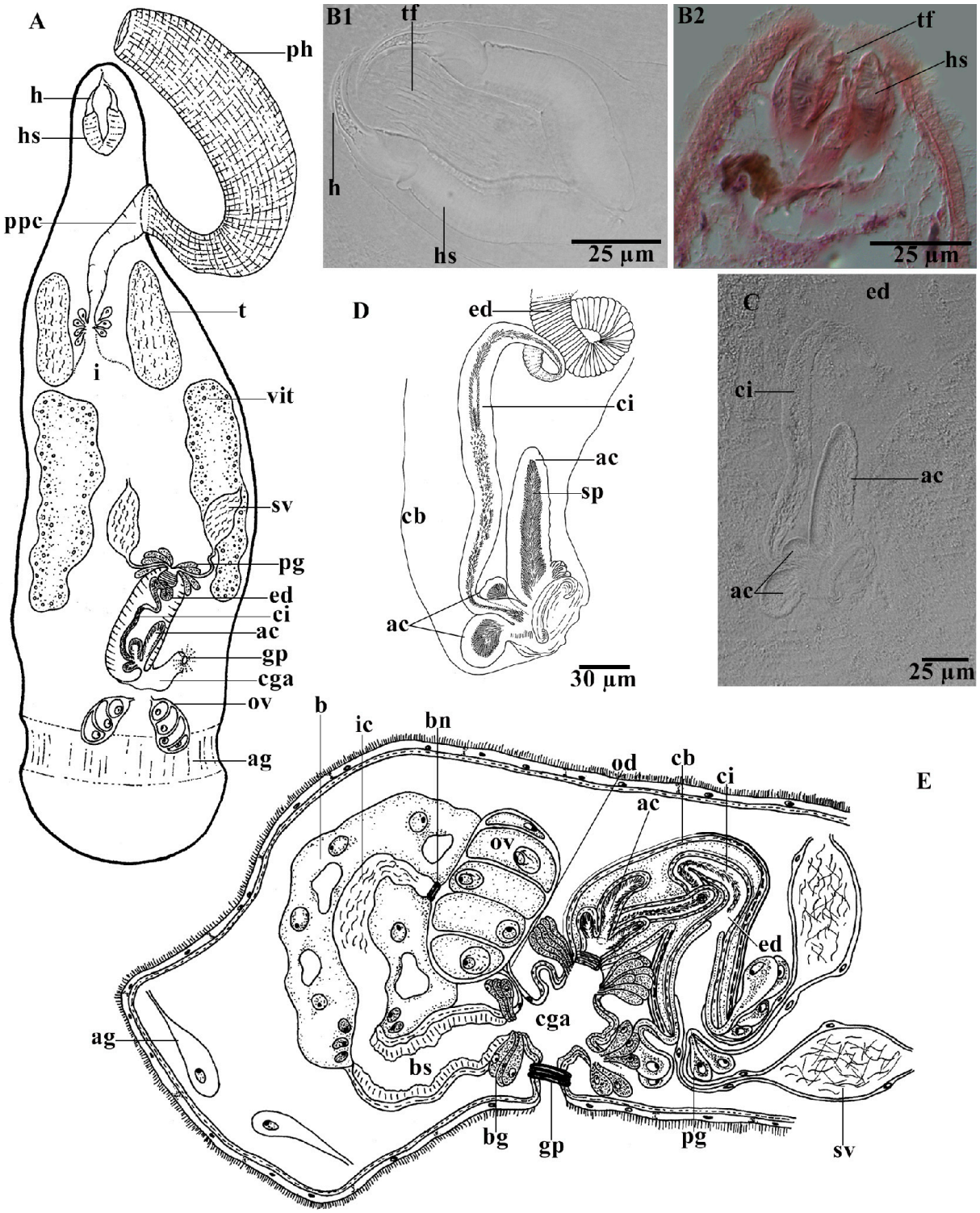


Figure 2. *Baltoplana tricirrata* n. sp. (**A**) General organisation (from a live specimen)—the pharynx protrudes from its cavity. (**B1**) Proboscis with hooks (from a whole mount). (**B2**) Proboscis with tactile fingers (from a histological section). (**C**) Photograph of the cirrus and the three accessory cirri. (**D**) Schematic representation of the cirrus and the accessory cirri ((**C**,**D**) from the holotype). (**E**) Reconstruction of the atrial organs from the right-hand side (only one ovary was depicted).

Male reproductive system: Two testes are located alongside the prepharyngeal cavity and the pharynx. The male copulatory bulb is situated in the posterior third of the body (Figure 2A). The proximal region of the bulb is lined with strong inner circular and outer longitudinal muscle fibres, which become weaker in the distal region (Figure 2E). The

paired seminal vesicles are surrounded by a low nucleated epithelium; muscles were not observed. The seminal vesicles narrow distally and fuse just anterior to the copulatory bulb, forming the ejaculatory duct (Figure 2A,C–E). Bundles of large extracapsular prostate glands, containing a fine-grained, basophilic secretion, enter the copulatory bulb proximally (Figure 2A,E). After entering the copulatory bulb, they discharge into the ejaculatory duct. The proximal part of the ejaculatory duct is wide and coils irregularly, lined by inner circular and outer longitudinal muscles (Figure 2E). At the posterior half of the bulb, the ejaculatory duct forms a cirrus, which is 195–222 µm long ($\bar{x}$ = 208 µm, n = 2) (Figure 2C,D). The cirrus bears 1–3-µm-long needle-like spines ($\bar{x}$ = 2 µm, n = 5) in its proximal region, oriented posteriorly, which increase to 6–9 µm long towards the distal end ($\bar{x}$ = 8 µm, n = 5). At the distal end of the cirrus, three blind, accessory cirri armed with needle-like spines of varying sizes are present: one is elongated, 80–86 µm long ($\bar{x}$ = 83 µm, n = 2), with 5–14 µm ($\bar{x}$ = 9 µm, n = 22) long spines. The other two are globular to oval, and measure 41–47 µm long ($\bar{x}$ = 44 µm, n = 2), with 7–12 µm long ($\bar{x}$ = 10 µm, n = 16) spines, and 26–30 µm long ($\bar{x}$ = 28 µm, n = 2), with 5–10 µm long ($\bar{x}$ = 7 µm, n = 13) spines (Figure 2A,C–E). The cirrus and the accessory cirri open into the distal part of the ejaculatory duct, discharging into the common genital atrium, which is lined with a low, anucleate epithelium and surrounded by inner circular and outer longitudinal muscles (Figure 2E). The distal region of the copulatory bulb is sclerotised with folds but does not form a cap covering the distal tip. The common genital atrium receives the male system anteriorly from the dorsal side (Figure 2E).

Female reproductive system: Two vitellaria are located at both sides of the body and extend from the posterior region of the pharynx to the posterior end of the body (Figure 2A). The ovaries are in the posterior third of the body and are connected to the common genital atrium via the oviducts, at least one independent oviduct was observed (Figure 2E). The oviducts are narrow, lined with a high, nucleate epithelium. The ovaries connect to the insemination ducts through sclerotised bursal nozzles. The insemination ducts are connected posteriorly to the bulbous bursa (Figure 2E). The bursa is located just behind the ovaries and is lined by a syncytial epithelium; muscles are lacking. The bursa connects to the bursal stalk, which is lined with a high, anucleate epithelium, showing a slightly striated appearance and surrounded by inner circular and outer longitudinal muscles (Figure 2E). The bursal stalk leads into the posterior part of the common genital atrium. The entrance of the bursal stalk into the genital atrium is surrounded by a large bundle of glands containing a coarse-grained, basophilic secretion (Figure 2E). The common genital atrium leads to the gonopore, which is surrounded by a strong sphincter (Figure 2E). The gonopore is located ventrally at the posterior end of the body at about 80% of the body length.

Baltoplana bipartita n. sp. Reyes, Jouk & Artois

urn:lsid:zoobank.org:act:6449C20E-911E-47A1-9432-36FC890E9A05

Figure 3

Type material: *Holotype*: Australia • One whole mount; Port Lincoln, Coffin Bay National Park, beneath Golden Island Lookout, small bay with coarse-grained sand and shell gravel, ca. 20 cm deep; −34.687778, 135.327139 (type locality); 8 December 2010; AHC37226.

Etymology: The species name refers to the appearance of the cirrus and accessory cirrus, divided into two parts in the copulatory organ (Latin: *bi* = "two" or "double", *partita* (feminine form of *partitus*) = "divided" or "splitted")

Diagnosis: Species of *Baltoplana* characterised by a male copulatory organ with a cirrus 143 µm long. Robust spines within the cirrus gradually decrease in length from the proximal (44 µm) to the distal (22 µm) end. Accessory spiny cirrus 124 µm long, with ~72-µm-long, robust spines extending from the proximal to the distal region.

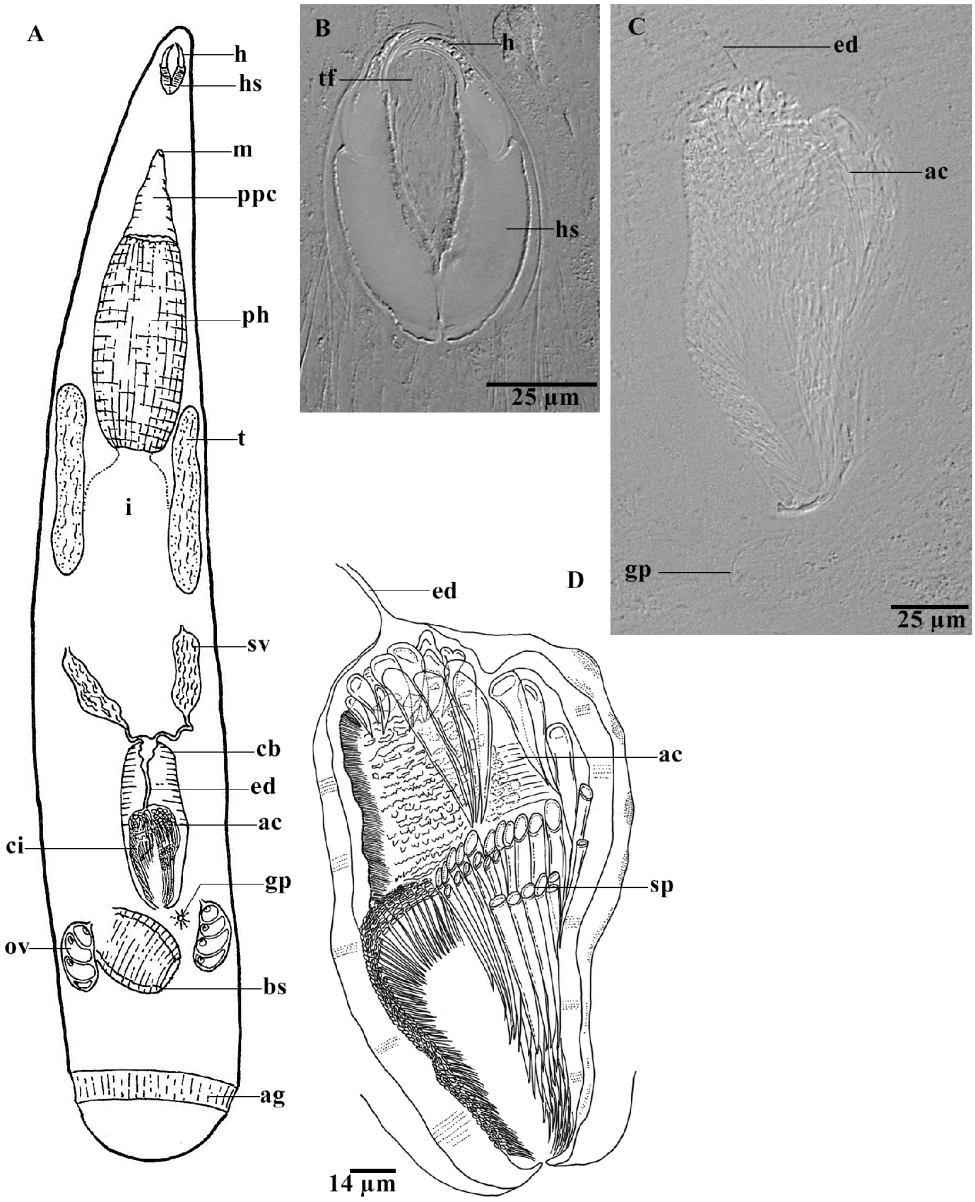


Figure 3. *Baltoplana bipartita* n. sp. (**A**) General organisation (from a live specimen). (**B**) Proboscis with hooks (from a whole mount). (**C**) Cirrus and accessory cirrus. (**D**) Schematic representation of the cirrus and accessory cirrus ((**C**,**D**) from the holotype).

Description: The fixed specimen is 2 mm long and 0.2 mm at its widest part. The proboscis is 111 µm long (Figure 3A), armed with 43 µm long hooks, without denticles (Figure 3B). The muscular hook supports are 47 µm long. Other general features as in *B. tricirrata* n. sp.

Male reproductive system: The paired seminal vesicles are in the middle section of the body, tapering distally to form seminal ducts that fuse just before entering the copulatory bulb, forming a long and slender ejaculatory duct (Figure 3A,C,D). The proximal part of the copulatory bulb is surrounded by robust muscles (Figure 3A). Proximally, the ejaculatory duct is widened and coiled (Figure 3A). At the copulatory bulb's midpoint, the ejaculatory duct turns into a cirrus that is 143 µm long. It has robust spines that gradually decrease in length from the proximal (44 µm) to the distal region (22 µm) (Figure 3A,C,D). Adjacent to the cirrus, there is a 124-µm-long accessory cirrus, which has 72-µm-long and robust spines extending to the distal area. Spines in the distal area are shorter, although their exact length could not be determined. (Figure 3C,D).

Female reproductive system: In the whole-mounted specimen, the ovaries are positioned at the posterior third of the body, next to the muscular bursal stalk (Figure 3A). The bursal stalk connects to the common genital atrium, which opens to the outside through the gonopore as in *B. tricirrata* n. sp.

Baltoplana floridana n. sp. Diez, Reyes & Artois

urn:lsid:zoobank.org:act:0C055333-0209-4B80-B02F-15623FD16D5B

Figure 4

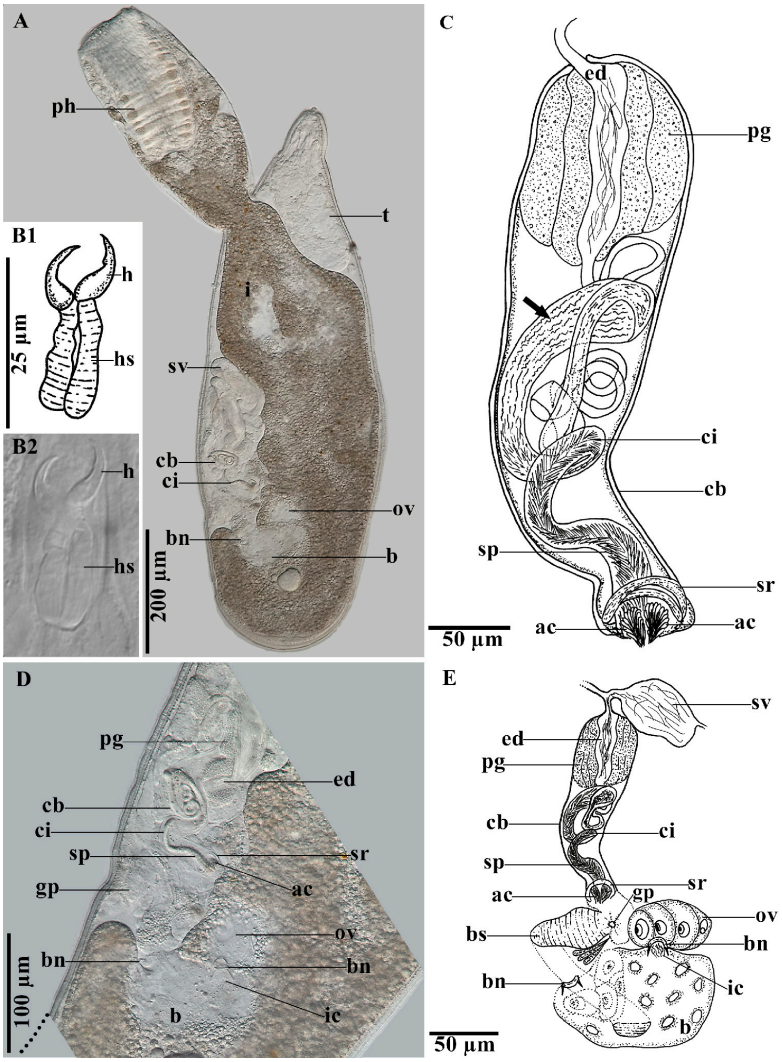


Figure 4. *Baltoplana floridana* n. sp. (**A**) General organisation from a live specimen—the pharynx protrudes from its cavity. (**B1**) Schematic representation of the proboscis hooks. (**B2**) Proboscis hooks with hooks support from a whole mount (same scale bar in (**B1**,**B2**)). (**C**) Schematic representation of the copulatory bulb, the zigzag ridges in the cirrus (arrow), the sclerotised ring, and the accessory cirri. (**D**) Photograph of the male and female copulatory system. (**E**) Schematic representation of the male and female copulatory systems.

Type material: *Holotype*: United States of America • One whole mount; Florida, Palm Beach, Jupiter, Carlin Park, intertidal, upper 10 cm of medium-coarse clean sand, salinity 35 ‰; 26.929561, −80.067744 (type locality); 26 April 2025; USNM 1783061.

Etymology: The specific epithet refers to the type locality in Florida.

Diagnosis: Species of *Baltoplana* with a 157-µm-long cirrus, which has zigzag-shaped sclerotised ridges in the proximal half, and 3–4-µm-long spines in its distal half. Two

11-µm-long, accessory cirri open into the distal part of the male duct, armed with 9-µm-long spines. Subterminal part of the copulatory bulb with a 21-µm-wide, sclerotised ring.

Description: The specimen measured 0.9 mm in length. The proboscis hooks are 11 µm long, supported by 17-µm-long muscular bases (Figure 4(A,B1,B2)).

Male reproductive system: The paired seminal vesicles are 149 µm long in the whole-mounted specimen, fusing distally before entering the male bulb. Extracapsular prostate glands open into the bulb from the proximal side. Within the bulb, the ejaculatory duct gradually widens proximally. The ejaculatory duct coils approximately three times before opening into the cirrus. The cirrus is 157 µm long, its proximal half is ornamented with zigzag-shaped sclerotised ridges, and the distal half is armed with 3–4-µm-long needle-like spines. At the distal aperture of the cirrus, two accessory cirri open, each measuring 11 µm in length (Figure 4C). The needle-like spines on the accessory cirri are broader than those on the cirrus, slightly curved and are 8–10 µm long ($\bar{x}$ = 9 µm, n = 10) (Figure 4C,D). A sclerotised, 21-µm-wide ring surrounds the distal part of the cirrus, it seems that do not form a cap.

Female reproductive system: The insemination ducts appear partially sclerotised (Figure 4D). The paired ovaries are connected to the bursa through sclerotised bursal nozzles (Figure 4D,E). The bursal stalk is lined, at least, by strong circular muscles (Figure 4E).

Baltoplana galerita n. sp. Jouk, Diez, Reyes & Artois

urn:lsid:zoobank.org:act:A811E296-42E9-45AC-A60B-6FD2475BC44E

Figure 5

Type material: *Holotype*: Spain • One whole mount; Portbou, northern Spain, beach near the quay towards the harbour, immediately alongside the quay at the water's edge, fine clean black sand; 42.426667, 3.162361 (type locality); 17 July 2015; KT.11435. *Paratypes*: Spain • Eight whole mounts; same locality and coordinates as for the holotype: one with the same collection data as for the holotype; HU IV.4.40; one collected ca. 2 m from the quay at the water's edge in the surf zone, coarse sand mixed with fine gravel; 5 May 2025; HU IV.4.41; one collected 2.5 m from the quay at the water's edge in the surf zone, fine clean black sand; 9 July 2019; HU IV.4.43; one collected ca. 2 m from the quay at the water's edge in the surf zone, coarse sand; 13 April 2011; HU IV.4.48; three collected at the water's edge in the surf zone, fine blackish sand with fine shell debris; 13 July 2009 (HU IV.4.49, HU IV.4.50) and 17 July 2009 (HU V.1.01); one collected 10–20 cm deep in fine blackish sand with shell grit; 3 September 2016; HU V.1.02. • Two histological sections; same locality and coordinates as for the holotype, collected 10–20 cm deep in fine blackish sand with shell grit; 3 September 2016; HU V.1.06, HU V.1.07. Italy • Three whole mounts; Sardinia, Torre del Porticciolo Beach, between rocks, at and above the waterline, fairly coarse sand with silt, to ca. 10 cm deep; 40.643806, 8.187306; 14 August 1994; HU IV.4.35, HU IV.4.36, HU IV.4.37. • Two whole mounts; Tuscany, Castiglione della Pescaia, subtidal, medium-grained sand, 0.5 m deep; 42.761358, 10.881319; 11 August 2024; HU IV.4.38, HU IV.4.39.

Additional material: Spain • Seven juvenile whole mounts; Portbou, northern Spain, beach near the quay towards the harbour; 42.426667, 3.162361: four collected 2.5 m from the quay at the water's edge in the surf zone, fine clean black sand; 9 July 2019; HU IV.4.42, HU IV.4.44, HU IV.4.45, HU IV.4.46; three collected 10–20 cm deep in fine blackish sand with shell grit; 3 September 2016; HU V.1.03, HU V.1.04, HU V.1.05; Four specimens kept for posterior molecular studies; same locality and coordinates as for the holotype; 17 July 2015; and paratype; 17 July 2009, 5 May 2025. France • One juvenile whole mount; southern France, Cerbère, beach in the city centre, 20 m left of the harbour wall, at the water's edge in the surf zone, coarse gravel with some larger pebbles and a small amount of silt; 42.442111, 3.166028; 5 April 2012; HU IV.4.47. Italy • Two specimens used for molecular analyses;

Tuscany, Castiglione della Pescaia, subtidal, medium-grained sand, 0.5 m deep; 42.761358, 10.881319; 11 August 2024.

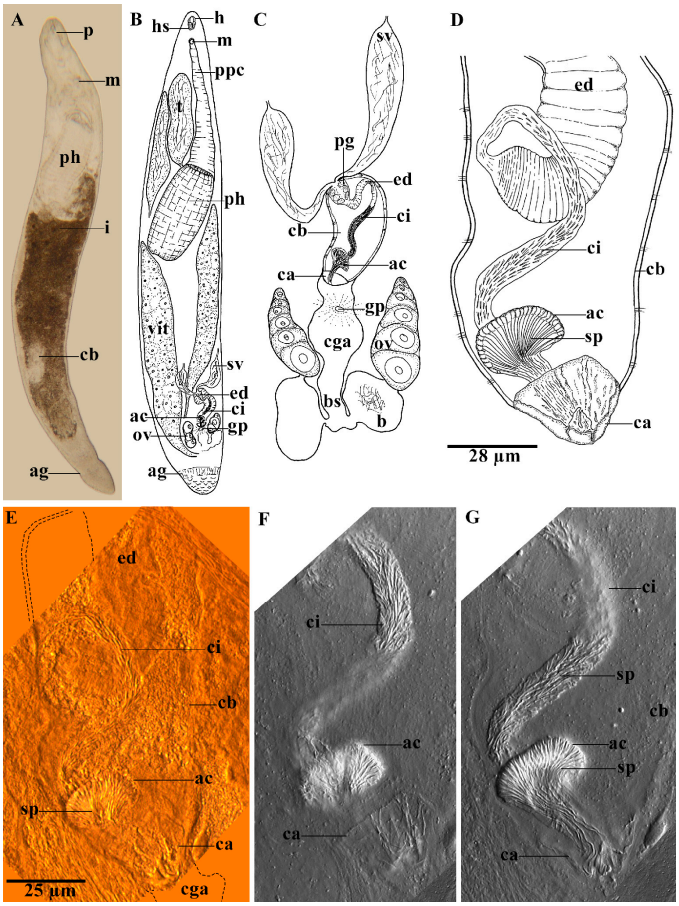


Figure 5. *Baltoplana galerita* n. sp. (**A**) General organisation (from a live specimen). (**B**) Schematic representation of a live specimen. (**C**) Schematic representation of the male and female reproductive systems (scale bar not available in (**A**–**C**)). (**D**) Schematic representation of the cirrus, the accessory cirrus, and the sclerotised cap. (**E**) Photograph of the cirrus, the accessory cirrus, and the sclerotised cap. (**F**,**G**) Detailed photograph of the cirrus and accessory cirrus in different focal planes (scale bar unavailable).

Etymology: The species name refers to the sclerotised cap of the male copulatory organ (Latin: *galeritus* = wearing a wool hat).

Diagnosis: Species of *Baltoplana* with a ~128-µm-long cirrus and a ~23-µm-long accessory cirrus, both with ~8-µm-long spines. Distal region of the copulatory bulb with a ~14 µm-long sclerotised cap, which represents ~11% of the length of the spiny cirrus.

Description: The live adult animals are 5–7 mm long and 0.5–1 mm wide (Figure 5A). The proboscis hook supports are 26–62 µm long ($\bar{x}$ = 43 µm, n = 34). The proboscis hooks are robust, 31–48 µm long ($\bar{x}$ = 37 µm, n = 33) (Figure 5A,B). The cylindrical pharynx is 222–710 µm long ($\bar{x}$ = 397 µm, n = 16) and 105–253 µm ($\bar{x}$ = 177 µm, n = 16) wide (Figure 5A,B). The pre-pharyngeal cavity is sinusoid when retracted (Figure 5A,B). A glandular mass (Minots's) surrounds the oesophagus.

Male reproductive system: The paired seminal vesicles narrow distally to form seminal ducts, which fuse just before entering the copulatory bulb (Figure 5B,C). The copulatory bulb is lined by inner longitudinal and outer circular muscles. The ejaculatory duct enters the elongated copulatory bulb through its anterior wall. It is widened at its proximal part, which is lined by circular muscles, and it runs centrally through the prostate vesicle (Figure 5C). Distally, the ejaculatory duct becomes a cirrus, which is 81–139 µm long ($\bar{x}$ = 128 µm, n = 8)

and possesses a sclerotised, strongly folded basal membrane that forms 5–12-µm-long needle-like spines ($\bar{x}$ = 8 µm, n = 15), protruding distally into the lumen (Figure 5D). Near the posterior end of this cirrus, a blind accessory cirrus opens (Figure 5D–G). This accessory cirrus has a sclerotised, strongly folded basal membrane forming ridges that project spines, 5–11 µm long ($\bar{x}$ = 8 µm, n = 14), into the lumen (Figure 5D,F,G). The accessory cirrus is 19–30 µm long ($\bar{x}$ = 23 µm, n = 8) and 23–31 µm wide ($\bar{x}$ = 26 µm, n = 8) (Figure 5D,E). Both cirri end in a slightly sclerotised cap that is 10–17 µm ($\bar{x}$ = 14 µm, n = 7) long and 32–49 µm wide ($\bar{x}$ = 38 µm, n = 8) covering the distal end of the copulatory bulb (Figure 5C–G). The length of the sclerotised cap represents ~11% of the length of the cirrus (Figure 5D–G).

Female reproductive system: Located in the posterior third of the body, the two ovaries are connected to the common genital atrium through delicate oviducts as in *B. magna*. These oviducts lack muscles and possess a high, nucleated epithelial lining. Sclerotised nozzles connect the ovaries to the bulbous bursa, via the insemination ducts. The bursa is positioned posterior to the ovaries. The bursal stalk opens into the common genital atrium, at the same point where it discharges a bundle of glands, containing a coarse-grained, basophilic secretion. A bundle of basophilic glands enters the common genital atrium ventrally.

Baltoplana magna Karling, 1949

Figure 6

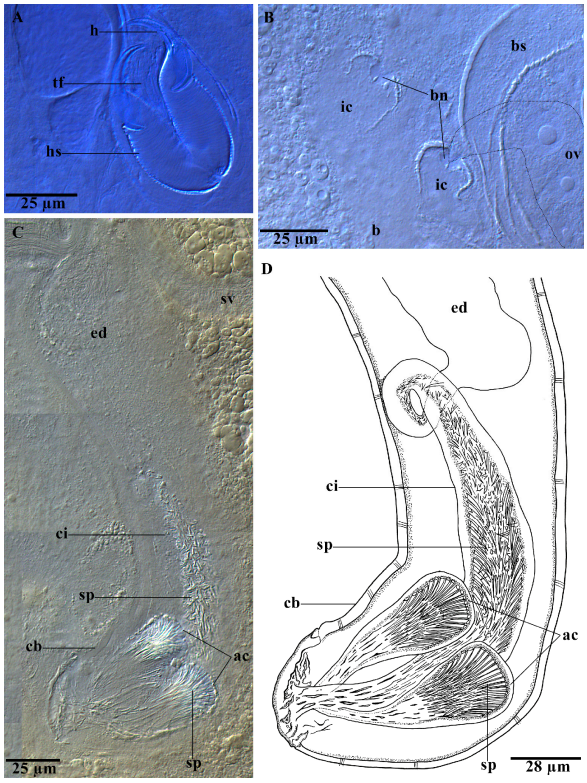


Figure 6. *Baltoplana magna* Karling, 1949. (**A**) Proboscis hooks. (**B**) Photograph of the female copulatory system—the dotted line indicates the ovary, which overlaps the bursal nozzle. (**C**) Photograph of the armed cirrus and the two accessory cirri. (**D**) Schematic representation of the distal region of the cirrus and the two accessory cirri.

Known distribution: The species was recorded from the Mediterranean and North America (New Elmtree River, Brunswick, Canada) [57], and from the European Atlantic coasts (North Sea and Baltic Sea; Great Britain, France; and San Antonio Beach, Spain) [13,17,58,59].

New material: France • Two whole mounts; Ambleteuse, near the sea, 70 m from the dike, sandy surface, salinity 30–35 ‰; 50.806417, 1.596972; 23 July 2015; HU XXVII.2.15—XXVII.2.16. One specimen used for DNA analysis.

Remarks: Habitus and internal organisation of the newly collected specimens are as described by Karling [13]. The fixed specimens are 1.3–1.5 mm long ($\bar{x}$ = 1.4 mm, n = 2) and 0.2–0.3 mm wide ($\bar{x}$ = 258 µm, n = 2) (Figure 6A). The 171-µm-long proboscis bears curved hooks, 30–43 µm long ($\bar{x}$ = 38 µm, n = 4). The muscular hook supports are 42–49 µm long ($\bar{x}$ = 44 µm, n = 4) (Figure 6A).

Male reproductive system: The copulatory bulb is situated in the posterior third of the body (Figure 6C,D). Two lateral seminal vesicles lie in the posterior body's third, narrow distally and fuse to form the ejaculatory duct, which enters the copulatory bulb proximally (Figure 6C). The ejaculatory duct makes a coil in its proximal part, where it is surrounded by the prostate vesicle. Distally, the ejaculatory duct forms a cirrus, 213–219 µm long ($\bar{x}$ = 216 µm, n = 2) and 17–23 µm wide ($\bar{x}$ = 20 µm, n = 2) (Figure 6C,D). The cirrus exhibits needle-like spines. The spines in the proximal part of the cirrus increase in length from 6 µm to 25 µm ($\bar{x}$ = 13 µm, n = 12), whereas in the distal part they are 3–5 µm long ($\bar{x}$ = 3 µm, n = 12) (Figure 6C,D). Two equally long accessory cirri open at the same level as the main cirrus into the male atrium, they are 52–79 µm long ($\bar{x}$ = 65 µm, n = 4). The accessory cirri bear needle-like spines 16–22 µm long ($\bar{x}$ = 18 µm, n = 6), which are larger in the proximal region and decrease in size towards the distal end (Figure 6C,D).

Female reproductive system: The ovaries are in the posterior body's third, connected to the bursa via sclerotised nozzles. The sclerotised nozzles are connected to the insemination ducts as described by Karling [13] (Figure 6B).

Baltoplana quadricirrata n. sp. Reyes, Schockaert, Monnens & Artois
urn:lsid:zoobank.org:act:707F9167-5F12-43FF-8963-C5B5FD00F075
Figure 7

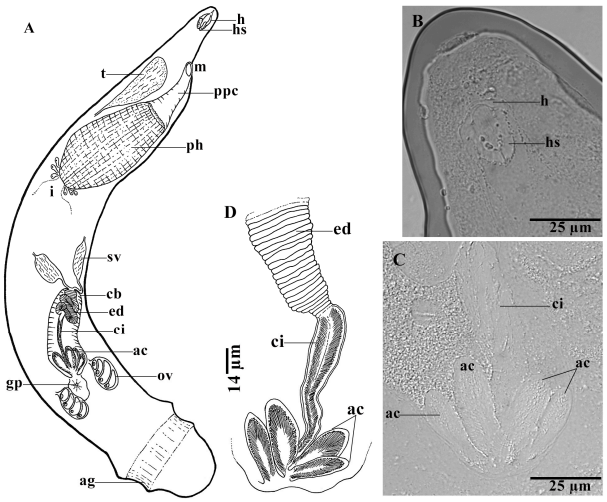


Figure 7. *Baltoplana quadricirrata* n. sp. (**A**) General organisation from a fixed specimen (only one testis depicted). (**B**) Proboscis with hooks (from a whole mount). (**C**) Photograph of the cirrus and the four accessory cirri. (**D**) Schematic representation of the cirrus and the four accessory cirri.

Type material: *Holotype*: Australia • One whole mount; New South Wales, Byron Bay, Coffs Harbour, mid-littoral, fine sand, 1–2 m deep; −28.642222, 153.619694 (type locality); 19 July 2003; W.60096.001. *Paratypes*: Australia • One whole mount; same data as for the holotype; HU V.1.10. • Two whole mounts; New South Wales, Broken Head Beach; −28.702139, 153.613917: one collected mid-eulittorally on an open beach south of the headland, fine sand and a large tidal pool with coarse sand; 27 October 1997; HU V.1.09;

one collected mid-littorally in fine sand in a sheltered area; 20 July 2003; HU V.1.11. • One whole mount; New South Wales, Lennox Head Beach, mid-eulittoral, relatively coarse sand in a fairly protected, lagoon-like pool with stones; −28.791139, 153.594528; 27 October 1997; HU V.1.08. • One whole mount; New South Wales, Campbell Beach, south of the bump, low-littoral, coarse surface sand; −30.242472, 153.147750; 17 July 2003; HU V.1.12.

Etymology: The species name refers to the number of accessory cirri of the male copulatory organ (Latin: *quadri*, derived from *quattuor* = four, and *cirratus*, an adjective derived from *cirrus*).

Diagnosis: Species of *Baltoplana* with a male copulatory organ with a ~93-µm-long cirrus and four accessory cirri measuring ~45 µm, ~37 µm, ~34 µm, ~26 µm. Spines in the cirrus are ~7 µm long. Proximal and distal spines are ~14 µm long and ~4 µm long, respectively, in all accessory cirri.

Description: The fixed animals are 0.8–2.5 mm long ($\bar{x}$ = 1.6 mm, n = 6) and 0.1–0.3 mm at their widest point ($\bar{x}$ = 0.2 mm, n = 6) (Figure 7A). Anterior body region with a small proboscis, 43–58 µm ($\bar{x}$ = 51 µm, n = 3) long (Figure 7A,B). The proboscis bears curved and slender hooks, which are 8–17 µm long ($\bar{x}$ = 13 µm, n = 10) (Figure 7B). The hooks are connected to the 6–26-µm-long muscular supports ($\bar{x}$ = 17 µm, n = 10) (Figure 7A,B).

Male reproductive system: Two seminal vesicles narrow gradually to fuse and form the ejaculatory duct, which enters the copulatory bulb proximally (Figure 7A,C,D). The ejaculatory duct gradually widens towards its proximal end and is coiled at its proximal part. At its distal region, it forms a 76–155-µm-long cirrus ($\bar{x}$ = 93 µm, n = 6) (Figure 7A,D). The cirrus is armed of 6–9 µm long ($\bar{x}$ = 7 µm, n = 5), needle-like spines (Figure 7D). At the distal end of the cirrus, four oval, accessory cirri of different length are present, two of which are slightly longer than the others (Figure 7C,D). The accessory cirri are 32–74 µm ($\bar{x}$ = 45 µm, n = 6), 26–52 µm ($\bar{x}$ = 37 µm, n = 6), 27–51 µm ($\bar{x}$ = 34 µm, n = 6) and 21–30 µm long ($\bar{x}$ = 26 µm, n = 6), respectively. The proximal and distal needle-like spines in the accessory cirri are 12–17 µm ($\bar{x}$ = 14 µm, n = 5) and 4–5 µm long ($\bar{x}$ = 4 µm, n = 5), respectively (Figure 7D).

Female reproductive system: Two ovaries are distinguished in live animals, like those described in *B. tricirrata* n. sp.

Baltoplana pseudovalkanovi n. sp. Reyes, Schockaert & Artois

urn:lsid:zoobank.org:act:F2DF7D94-CDB5-4C13-9E85-EF8304F6B5D6

Figure 8

Type material: *Holotype*: Brazil • One whole mount; São Paulo, São Sebastião, Toque Toque Grande Beach, near a river outlet, fine sand; −23.831417, −45.512639 (type locality); 15 June 2010; KT.11436. *Paratypes*: Brazil • One whole mount; São Paulo, São Sebastião, Toque Toque Grande Beach, near a river outlet, fine sand; −23.831472, −45.513167; 18 June 2010; HU V.1.13. • Three histological sections; one with the same data as for the holotype; HU V.1.16; two with the same data as for the whole-mounted paratype; HU V.1.14, HU V.1.15.

Other material: Brazil • Six specimens used for molecular analyses with the same data as for the paratype.

Etymology: The species name refers to the similarity of the reproductive system to that of *B. valkanovi* (Greek: ψευδή, pseudés, pseudo = false).

Diagnosis: Species of *Baltoplana* with a ~144-µm-long and ~20-µm-wide cirrus. Cirrus armed of ~12-µm-long spines proximally and ~6-µm-long spines distally. Without accessory cirri.

Description: The whole-mounted animals are 0.6–1.1 mm long ($\bar{x}$ = 0.9 mm, n = 2) and 0.1–0.2 mm at widest point ($\bar{x}$ = 0.1 mm, n = 2). The proboscis hooks are robust,

measuring 16–37 µm long ($\bar{x}$ = 26 µm, n = 4) (Figure 8A). The muscular hook supports of the proboscis are 17–45 µm long ($\bar{x}$ = 31 µm, n = 4) (Figure 8A).

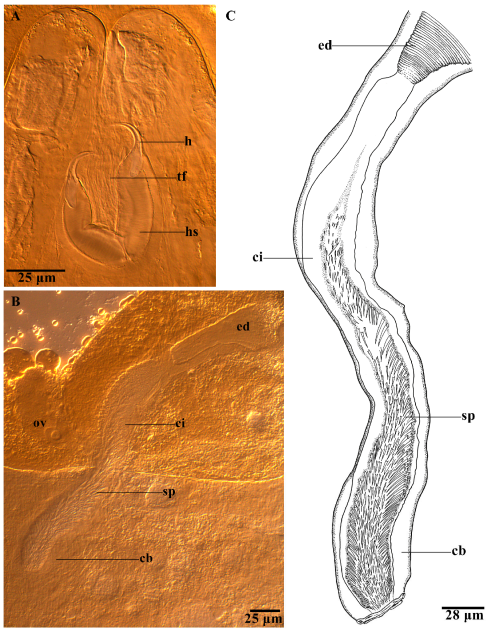


Figure 8. *Baltoplana pseudovalkanovi* n. sp. (**A**) Proboscis with hooks (from a whole mount). (**B**) Photograph of the cirrus. (**C**) Schematic representation of the cirrus.

Male reproductive system: Two testes observed in live animals. The paired seminal vesicles narrow distally to seminal ducts, which fuse before entering proximally the 336-µm-long copulatory bulb (n = 1) (Figure 8B). The ejaculatory duct runs centrally through the prostatic vesicle, located in the proximal part of the bulb. Distally, the ejaculatory duct becomes a cirrus with a sclerotised, strongly folded basal membrane that forms posteriorly projecting needle-like spines (Figure 8B,C). The cirrus is 72–216 µm long ($\bar{x}$ = 144 µm, n = 2) and 12–29 µm wide ($\bar{x}$ = 20 µm, n = 2). The proximal region of the cirrus is ornamented with 5–21-µm-long needle-like spines ($\bar{x}$ = 12 µm, n = 11), which are longer than those in the distal region [3–10 µm long ($\bar{x}$ = 6 µm, n = 11)] (Figure 8B,C). Some pseudosclerotised tissue is present in the distal region of the copulatory bulb, but it does not form a cap. There are no accessory cirri.

Female reproductive system: The ovaries are connected to the bulbous bursa through sclerotised nozzles. The sclerotised nozzles are connected to the insemination ducts and are partially immersed into the bursa. Other female structures are as those in *B. magna* [13].

Baltoplana brusai n. sp. Reyes, Schockaert & Artois

urn:lsid:zoobank.org:act:D224D900-35B6-44D8-B43A-8C86B1CBA76F

Figure 9

Type material: *Holotype*: Brazil • One whole mount; São Paulo, São Sebastião, Toque Toque Grande Beach, near a river outlet, fine sand; −23.831417, −45.512639 (type locality); 10 June 2010; KT.11437.

Etymology: Species named after Dr Francisco Brusa (Universidad Nacional de La Plata, División Zoología Invertebrados, Facultad de Ciencias Naturales y Museo, La Plata, Argentina), a prominent and generous Argentinian researcher, for his outstanding contribution to the knowledge of turbellarians.

Diagnosis: Species of *Baltoplana* with a 70-µm-long cirrus, with 9-µm-long spines in the proximal and middle regions, and 5 µm long spines distally. Distal region of the copulatory bulb with a 12 µm-long sclerotised cap that represents 18% of the length of the cirrus. No accessory cirri.

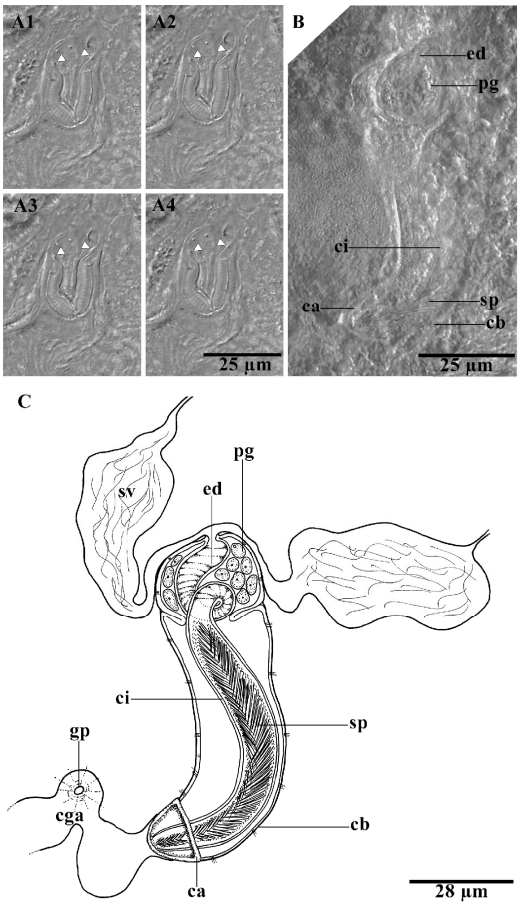


Figure 9. *Baltoplana brusai* n. sp. (**A1**–**A4**) Proboscis hooks with two denticles in different focal planes (white arrowheads). (**B**) Photograph of the cirrus and the sclerotised cap (from the holotype). (**C**) Schematic representation of the cirrus and the sclerotised cap.

Description: The fixed specimen is 0.9 mm long and 0.1 mm at its widest. Its anterior end with a 78-µm-long proboscis. The slender, curved proboscis hooks are 18–19 µm long ($\bar{x}$ = 18.5 µm, n = 2) and are smooth but with two denticles on their internal side (Figure 9A). The muscular hook supports are 18–21 µm long ($\bar{x}$ = 20 µm, n = 2) (Figure 9(A1–A4)).

Male reproductive system: The 91-µm-long copulatory bulb is in the posterior third of the body (Figure 9B). The paired seminal vesicles taper to seminal ducts that merge just before entering the copulatory organ, forming a long cirrus (Figure 9B,C). Proximally into the bulb, the duct widens and makes a coil (Figure 9B,C). The proximal part of the bulb contains the prostate vesicle, the glands of which discharges into the ejaculatory duct. The ejaculatory duct transitions into a cirrus, 70 µm long and 7 µm at its widest. The needle-like spines of the cirrus are longer in the proximal and middle regions (8–11 µm, $\bar{x}$ = 9 µm, n = 12), and gradually become shorter in the distal region (3–7 µm, $\bar{x}$ = 5 µm, n = 12) (Figure 9B,C). The cirrus tapers distally towards the distal end of the copulatory bulb. The distal end of the copulatory bulb shows a sclerotised cap, 12 µm long and 16 µm wide (Figure 9B,C). The length of the sclerotised cap represents ~18% of the length of the spiny cirrus (Figure 9C).

Female reproductive system: Only the ovaries positioned in the posterior third of the body were observed.

Baltoplana valkanovi Ax, 1959

Figure 10

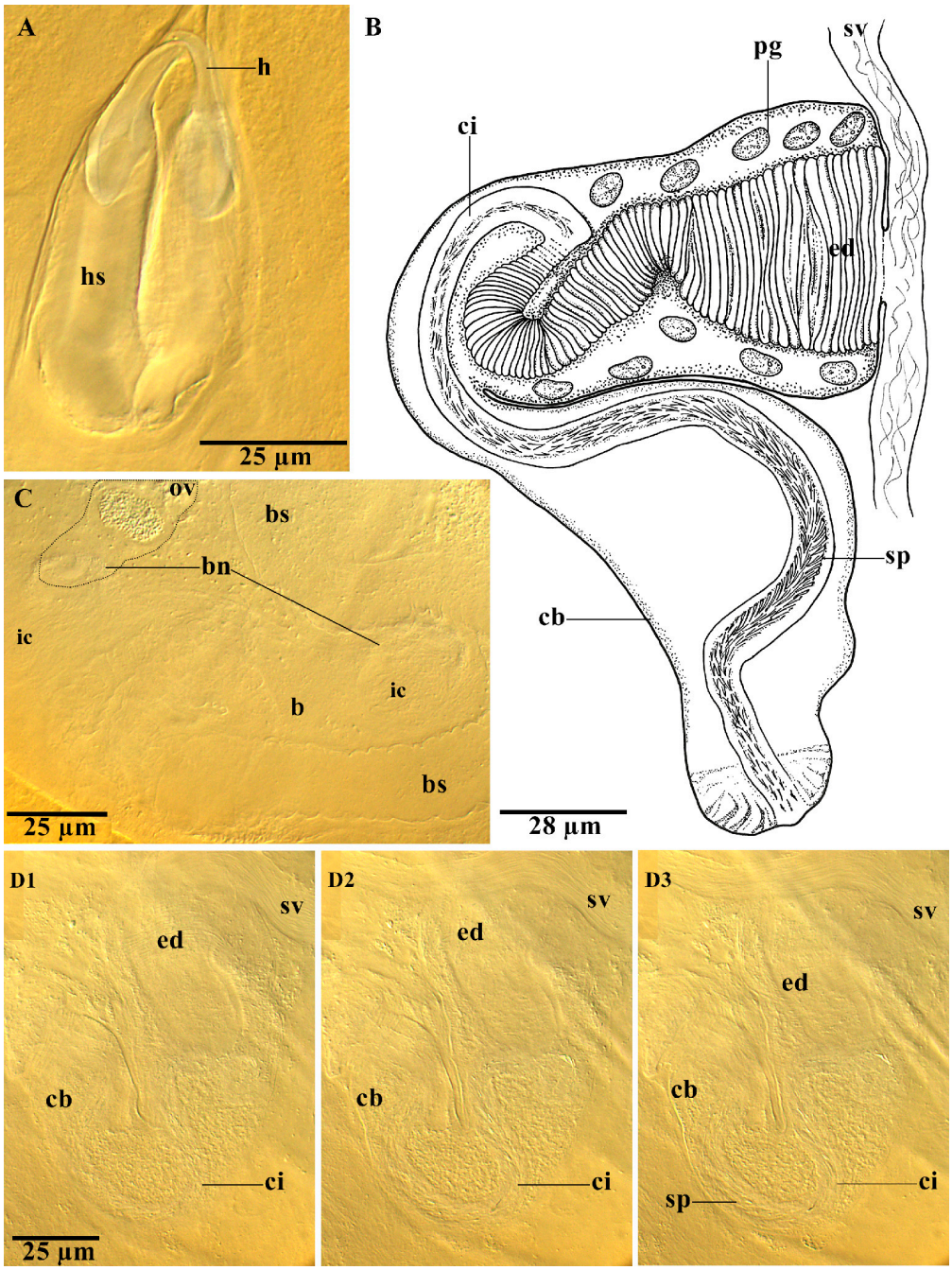


Figure 10. *Baltoplana valkanovi* Ax, 1959. (**A**) Proboscis hooks. (**B**) Schematic representation of the copulatory organ and the armed cirrus. (**C**) Photograph of the female copulatory system—the dotted line indicates the ovary, which overlaps the bursal nozzle. (**D1–D3**) Detailed photograph of the armed cirrus in different focal planes (same scale bar for photos 1, 2, and 3).

Known distribution: Black Sea: Poyraz, Turkey, and Varna, Bulgaria [15,60].

New material: Italy • One whole mount; Sardinia, Cala Tonda, littoral, 1–1.5 m deep; 41.062833, 8.290278; 23 September 2010; HU XXVII.2.17. • One whole mount; Sardinia, Cala d'Arena, intertidal, 0.3–4 m deep; 41.106500, 8.322778; 30 September 2014; HU XXVII.2.18. • One specimen used for molecular analyses; same data as for the previous specimen. • One whole mount; Sardinia, Cala del Bianco, intertidal, 2.5 m deep; 41.073861, 8.336611; 25 September 2014; HU XXVII.2.19. • One whole mount; Sardinia, Cala del Bianco, coarse sand, 6 m deep; 41.074417, 8.338222; 25 September 2014; HU XXVII.2.20.

Remarks: The habitus and internal organisation of the newly collected specimens are as described by Ax [15]. The fixed animals are 0.8–1.4 mm long ($\bar{x}$ = 1.1 mm, n = 4) and 0.2–0.4 mm wide ($\bar{x}$ = 0.3 mm, n = 4). The proboscis hooks are 34–39 µm long ($\bar{x}$ = 37 µm, n = 6) and the muscular supports 33–55 µm long ($\bar{x}$ = 47 µm, n = 6) (Figure 10A).

Male reproductive system: The paired seminal vesicles narrow distally to seminal ducts, which fuse before entering the 166–173 µm long ($\bar{x}$ = 169 µm, n = 4) copulatory bulb (Figure 10B,D). The ejaculatory duct is wide at its proximal end and narrows in its posterior part to form a cirrus, carrying needle-like spines posteriorly (Figure 10(B,D1–D3)). The cirrus is 189–246 µm long ($\bar{x}$ = 216 µm, n = 4) and 5–9 µm wide ($\bar{x}$ = 6 µm, n = 4). The spines are smaller (~1–2 µm long) in the proximal region of the cirrus, increasing in size towards the middle region [5–9 µm long ($\bar{x}$ = 7 µm, n = 20)], and slightly decreasing in size in the distal region, 3–8 µm long ($\bar{x}$ = 5 µm, n = 20) (Figure 10B). Some specimens present sclerotised tissue in the distal region of the copulatory bulb, but this does not form a cap (Figure 10B).

Female reproductive system: The ovaries are connected to a bursa by sclerotised nozzles, and the bursa empties into the bursa stalk (Figure 10C). Other female structures are as described by Ax [15].

Table 4 compares the diagnostic characters across the eleven species now assigned to *Baltoplana*, including the two known only from the literature. The habitus, the pharynx, the proboscis apparatus and the female reproductive system take almost the same state throughout the genus, so that the whole of the interspecific signal resides in the male copulatory organ. These are the characters on which the identification key in Section 5.2 is built.

4.2. Phylogenetic Relationships Within Cheliplanidae—Baltoplana

The analysed datasets had an extension of 1934 bp and 1809 bp for 18S and 28S rDNA partial genes, respectively (concatenated dataset of 3743 bp). The BI and ML inference analyses based on concatenated 18S and 28S rDNA recovered identical topologies after collapsing branches with low support and are summarised in Figure 11. The corresponding uncollapsed trees are provided as Figures S1–S3.

Three major clades are recovered within Schizorhynchia: one containing species of Diascorhynchidae, Karkinorhynchidae, and most 'Schizorhynchidae' (excluding *Carcharodorhynchus*) (SH-aLRT = 99.6, UFboot = 100, pp = 1), another encompassing both species of *Carcharodorhynchus* (SH-aLRT = 100, UFboot = 100, pp = 1), and a third group including all species of Cheliplanidae (SH-aLRT = 100, UFboot = 100, pp = 1). Within the first group of species, a clade formed by species of *Pseudoschizochilus* and *Schizorhynchoides* (SH-aLRT = 98.1, UFboot = 98, pp = 1) is the sister clade of a clade containing all other species (SH-aLRT = 89.8, UFboot = 96, pp = 0.99) (Figure 11).

Within Cheliplanidae, *Baltoplana galerita* n. sp. (two specimens forming a monophyletic clade; SH-aLRT = 100, UFboot = 100, pp = 1), is the sister taxon of a clade encompassing all other species of Cheliplanidae (SH-aLRT = 99.5, UFboot = 100, pp = 1) (Figure 11). The latter consists of a trichotomy of *B. magna* + *C. caudata* (SH-aLRT = 98.7, UFboot = 99, pp = 0.99), *Cheliplana boadeni* + *C. remanei* (SH-aLRT = 96.9, UFboot = 99, pp = 1), and a clade consisting of all the remaining species of *Cheliplana* (SH-aLRT = 100, UFboot = 100, pp = 1). Within the subclade containing most species of *Cheliplana*, *C. cubana* + *C. curacaoensis* (SH-aLRT = 99.3, UFboot = 99, pp = 1) is the sister group to *C.* cf. *orthocirra* + *C. subproximalis* + *C. terminalis* (SH-aLRT = 94.9, UFboot = 96, pp = 1). *Cheliplana subproximalis* and *C. terminalis* are more closely related (SH-aLRT = 95.9, UFboot = 100, pp = 1).

Table 4. Comparative matrix of the diagnostic characters of the eleven species of *Baltoplana*. Measurements are given as mean (range) when more than one specimen or structure was measured, and as a single value when $n = 1$. Species described in this study are marked n. sp. "?", not known; "–", not applicable.

Character	***B. bipartita* n. sp.**	***B. bisphaera***	***B. brusai* n. sp.**	***B. cupressus***	***B. floridana* n. sp.**	***B. galerita* n. sp.**	***B. magna***	***B. pseudovalkanovi* n. sp.**	***B. quadricirrata* n. sp.**	***B. tricirrata* n. sp.**	***B. valkanovi***
Habitus and proboscis											
Type locality/known distribution	Australia (Coffin Bay)	Kenya (Tudor Creek, Mombasa)	Brazil (São Paulo)	South Africa (KwaZulu-Natal)	USA (Florida)	Spain (Portbou)	Mediterranean and European Atlantic coasts [13,14]	Brazil (São Paulo)	Australia (New South Wales)	Australia (Coffin Bay)	Black Sea (Poyraz; Varna)
Body length (mm)	2	1.7	0.9	1–1.4	0.9	5–7	1.4 (1.3–1.5)	0.9 (0.6–1.1)	1.6 (0.8–2.5)	1.6 (0.9–2.6)	1.1 (0.8–1.4)
Proboscis hook length (µm)	43	28–30	18.5 (18–19)	29 (24–33)	11	37 (31–48)	38 (30–43)	26 (16–37)	13 (8–17)	44 (41–46)	37 (34–39)
Denticles on proboscis hooks	absent	absent	present (2, internal side)	present (small)	absent	absent	absent	absent	absent	absent	absent
Male copulatory organ											
Copulatory bulb length (µm)	?	ca. 180	91	?	?	?	?	336	?	?	169 (166–173)
Proximal coil of ejaculatory duct	present (1)	not reported	present (1)	?	present (ca. 3 coils)	present (1)	present (1)	not reported	present (1)	present (irregular)	not reported
Cirrus (spiny, sclerotised)	present	absent (duct unarmed)	present	present	present	present	present	present	present	present	present
Cirrus length (µm)	143	–	70	23 (20–26)	157	128 (81–139)	216 (213–219)	144 (72–216)	93 (76–155)	208 (195–222)	216 (189–246)
Cirrus width (µm)	?	–	7	18 (16–19)	?	?	20 (17–23)	20 (12–29)	?	?	6 (5–9)
Additional cirrus ornamentation	robust spines	–	none	none	zigzag sclerotised ridges (proximal half)	none	none	none	none	none	none
Cirrus spines, proximal (µm)	44	–	9 (8–11)	?	absent (ridges only)	8 (5–12)	13 (6–25)	12 (5–21)	7 (6–9)	2 (1–3)	1–2
Cirrus spines, middle (µm)	–	–	9 (8–11)	?	–	8 (5–12)	–	–	7 (6–9)	–	7 (5–9)
Cirrus spines, distal (µm)	22	–	5 (3–7)	?	3–4	8 (5–12)	3 (3–5)	6 (3–10)	7 (6–9)	8 (6–9)	5 (3–8)
Trend of cirrus spine length (proximal → distal)	decreasing	–	decreasing	?	spines only distally	±uniform	decreasing	decreasing	±uniform	increasing	small–large–intermediate

Table 4. *Cont.*

Character	*B. bipartita* n. sp.	*B. bisphaera*	*B. brusai* n. sp.	*B. cupressus*	*B. floridana* n. sp.	*B. galerita* n. sp.	*B. magna*	*B. pseudovalkanovi* n. sp.	*B. quadricirrata* n. sp.	*B. tricirrata* n. sp.	*B. valkanovi*
Accessory cirri											
Number of accessory cirri	1	2	0	1	2	1	2	0	4	3	0
Accessory cirrus length (µm)	124	?	–	23 (19–26)	11; 11	23 (19–30)	65 (52–79); both equal	–	45 (32–74); 37 (26–52); 34 (27–51); 26 (21–30)	83 (80–86); 44 (41–47); 28 (26–30)	–
Accessory cirrus shape	elongate, bipartite	spherical	–	elongate	short, oval	blind, 26 (23–31) µm wide	spherical, equal	–	oval, unequal	1 elongate + 2 globular–oval	–
Accessory cirrus spines (µm)	72 (shorter distally)	?	–	?	9 (8–10), broad, curved	8 (5–11)	18 (16–22), larger proximally	–	14 (12–17) proximal; 4 (4–5) distal	9 (5–14); 10 (7–12); 7 (5–10)	–
Distal sclerotisation of the copulatory bulb											
Type of distal sclerotisation	absent	absent	cap	absent	subterminal ring (no cap)	cap	absent	diffuse, no cap	absent	folds, no cap	diffuse (some specimens), no cap
Cap/ring dimensions (µm)	–	–	12 long × 16 wide	–	21 wide	14 (10–17) long × 38 (32–49) wide	–	–	–	–	–
Cap length: cirrus length (%)	–	–	ca. 18	–	–	ca. 11	–	–	–	–	–
Reference	this study	[16]	this study	[18]	this study	this study	[13]; this study	this study	this study	this study	[15]; this study

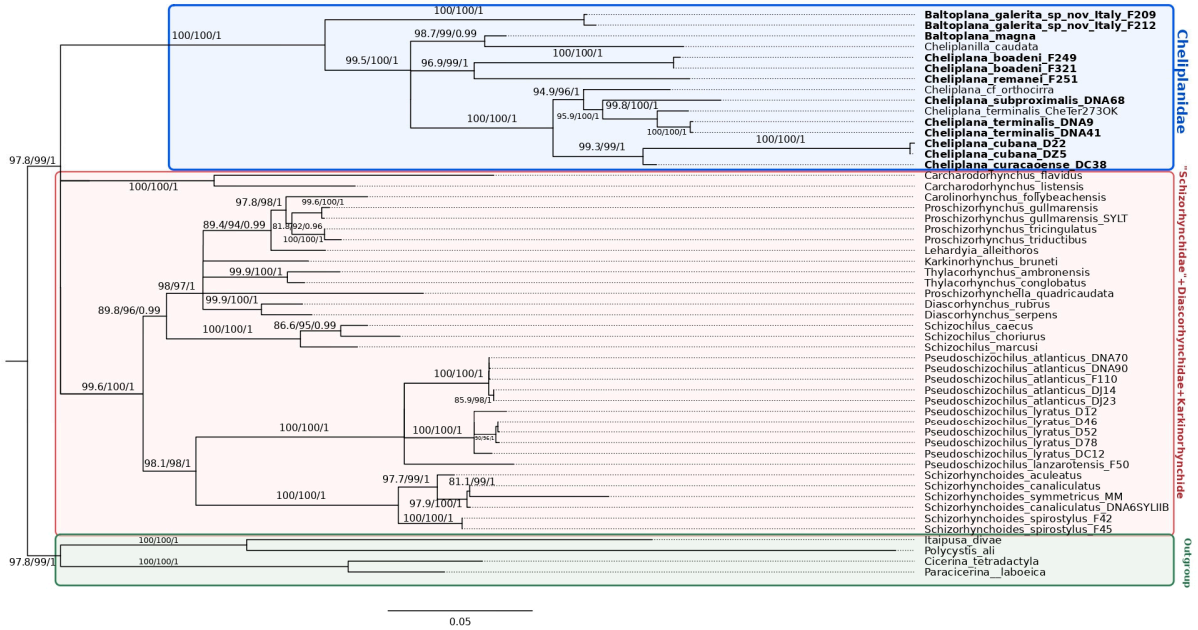


Figure 11. Phylogenetic relationships of species of *Baltoplana* inferred from concatenated 18S and 28S rDNA. The topology corresponds to the Bayesian inference analysis. Nodal support values are given in the order SH-aLRT/UFboot/pp, where SH-aLRT is the Shimodaira–Hasegawa-like approximate likelihood-ratio test (%), UFboot is the ultrafast bootstrap approximation (%), and pp is the Bayesian posterior probability. Branches with low support values SH-aLRT < 80, UFboot < 90, or pp < 0.95 are collapsed. New sequences are shown in bold. The uncollapsed trees, with support values at every node, are provided as Figures S1–S3.

The additional assessment of whether the genus *Baltoplana* is monophyletic showed that both analyses that combined the two datasets (combined 18S–28S), imposing the monophyly of *Baltoplana*, led to a decline in log-likelihood (ΔLogL = 49.995) (*p*-values listed in Table 5). All three tests (Kishino–Hasegawa, KH; Shimodaira–Hasegawa, SH; and Approximately Unbiased, AU) rejected the constrained topology ($p < 0.001$; Table 5). In the 18S-only analysis, the likelihood of the constrained topology was also lower than that of the unconstrained maximum-likelihood tree (ΔLogL = 53.106), and it was rejected by all statistical tests (KH, SH and AU) (*p*-values listed in Table 5). In contrast, the unconstrained maximum-likelihood analyses recovered *Cheliplana* as monophyletic in both molecular datasets. In the concatenated 18S–28S analysis, all seven species of *Cheliplana* (and their isolates) formed a monophyletic group. Enforcing the monophyly of *Cheliplana* recovered exactly the same branching order as the unconstrained search: the two trees are topologically identical and differ only in branch-length optimisation. The associated log-likelihood difference is accordingly negligible (ΔLogL = 0.0004), and none of the three tests rejected it (Table 5). In the 18S-only analysis, all seven species of *Cheliplana* (10 isolates) represented in the matrix also formed a monophyletic group, and the constrained and unconstrained trees were again topologically identical. The two representations differed by only 0.0003 log-likelihood units, with the constrained tree producing the marginally higher value, and the constrained topology was not rejected by the KH, SH, or AU tests (Table 5). Thus, the available molecular data recovered *Cheliplana* as monophyletic. Because the paired trees were topologically identical, the minute log-likelihood differences reflect numerical branch-length optimisation rather than differences in topology.

Table 5. Topology test results for the monophyly of *Baltoplana* and *Cheliplana* based on the concatenated partial 18S and 28S datasets, and the 18S-only dataset. Log-likelihood (LogL) values of the unconstrained maximum-likelihood tree and the genus-specific constrained trees, absolute log-likelihood differences (ΔLogL), and *p*-Values of the Kishino–Hasegawa (KH), Shimodaira–Hasegawa (SH), and Approximately Unbiased (AU) tests shown. Trees were considered significantly different when *p*-values were less than 0.05. Rejection of the constrained topology was interpreted as evidence that the current circumscription of the corresponding genus is incompatible with the topology recovered from the sampled taxa in that molecular dataset. Where the constrained and unconstrained trees are topologically identical (*Cheliplana*), the reported ΔLogL reflects numerical branch-length optimisation only.

Genus	Analysis	Unconstrained ML Tree LogL	Constrained Tree LogL	ΔLogL	KH (*p*-Value)	SH (*p*-Value)	AU (*p*-Value)
Baltoplana	Concatenated 18S–28S	−29,571.691	−29,621.686	49.995	0.0004	0.0004	0.0000635
	18S-only	−11,724.228	−11,777.333	53.106	0.0001	0.0001	0.000285
Cheliplana	Concatenated 18S–28S	−29,571.94344	−29,571.94384	0.0004	0.482	0.482	0.476
	18S-only	−11,729.34039	−11,729.34010	0.0003	0.516	1.000	0.512

4.3. Partial Mitochondrial Genome Annotations—Baltoplana valkanovi

Sequencing and assembly: Illumina sequencing produced a total of 22,365,194 paired-end reads of 151 bp, corresponding to 11,182,597 read pairs. NOVOPlasty successfully generated a 7154 bp mitochondrial contig, with an estimated average organellar coverage of 705×. About 0.34% of the reads contributed to the mitochondrial assembly. Although the assembler initially suggested that the contig was circular, biological confirmation of this circularity was not supported by the read data. As a result, the contig is conservatively described as a linear, partial mitochondrial sequence. It also contains nine ambiguous nucleotides, none of which are located within the validated gene annotations. The nucleotide composition is predominantly AT-rich (65.95%) and a GC content of 34.05%.

Partial mitochondrial architecture and validated gene content: The confirmed partial mitochondrial annotation included four protein-coding genes (PCGs): *cox1*, *atp6*, *nad1*, and *cob*, along with three transfer RNA genes, *trnQ*, *trnF*, and *trnI* (Table 6, Figure 12). All seven genes were positioned on the same strand. Collectively, these validated features spanned 4477 bp, constituting 62.6% of the assembled contig. The four PCGs contributed a total of 4269 bp, while the three tRNAs contributed 208 bp. The assembled partial mitochondrial contig has been deposited in GenBank under accession number PZ818244.

Table 6. Validated features in the partial mitochondrial contig of *Baltoplana valkanovi*. Coordinates refer to the final 7154-bp linear representation. Protein-coding genes were translated using NCBI translation Table 9. The genes are encoded in the same 5′ → 3′ orientation as in the deposited contig (GenBank accession PZ818244). The *cox1* initiation codon is inferred from an uninterrupted open reading frame and is reported as putative; the true 5′ boundary of *cox1* remains uncertain.

Gene	Coordinates	Length (bp)	Start–Stop/Anticodon	Product Length
trnQ	604–670	67	TTG	—
atp6	2020–2703	684	ATG–TAA	227 aa
nad1	2704–3576	873	ATG–TAA	290 aa
cob	3580–4719	1140	ATC–TAA	379 aa
trnF	4721–4790	70	GAA	—
cox1	5117–6688	1572	TTG (putative)–TAG	523 aa
trnI	6742–6812	71	GAT	—

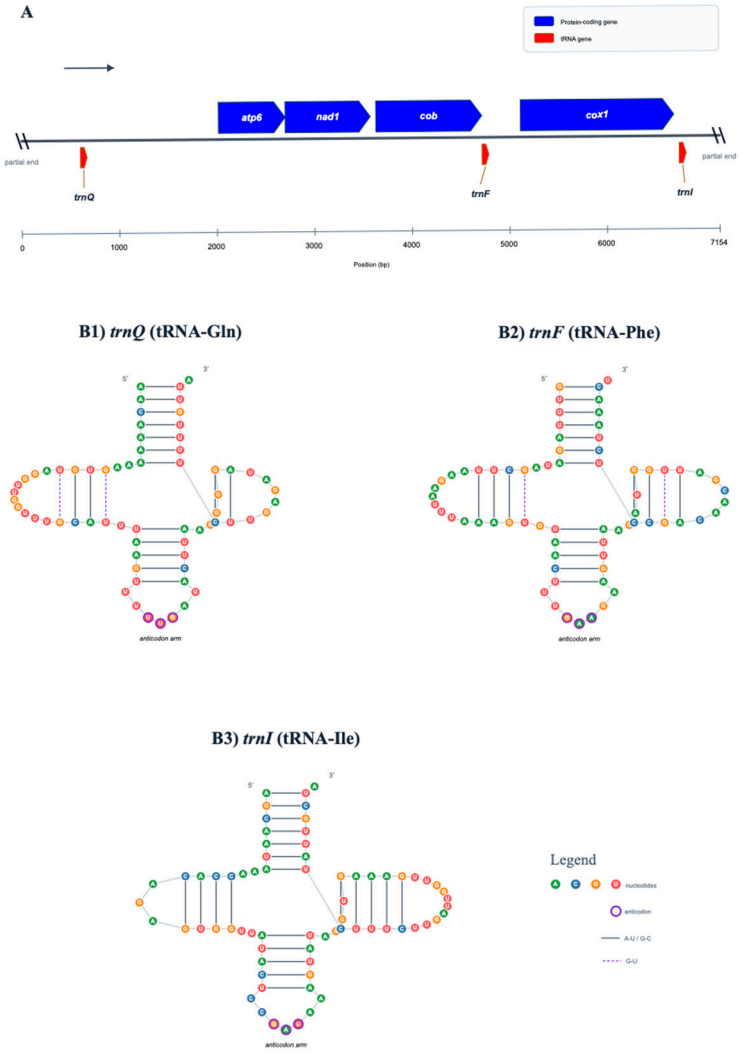


Figure 12. The linear representation and the predicted secondary structures of the partial mitochondrial genome and tRNAs of *Baltoplana valkanovi*, respectively. (**A**) The 7154-bp assembly contains four validated protein-coding genes (*atp6*, *nad1*, *cob*, and *cox1*) and three mitochondrial tRNA genes (*trnQ*, *trnF*, and *trnI*). Arrows indicate transcriptional orientation (5′ → 3′); all validated features are encoded on the plus strand. Unannotated regions are represented by the intervening line. The diagram does not imply genome circularity or completeness. (**B1**) trnQ (UUG), (**B2**) trnF (GAA), and (**B3**) trnI (GAU). Structures were reconstructed from tRNAscan-SE 2.0 organellar-mode predictions and manually checked against the corresponding genomic sequences. Anticodon nucleotides are outlined in purple. Solid lines indicate canonical A–U and G–C base pairs, purple dashed lines indicate G–U wobble pairs.

The confirmed arrangement of genes in the final linear representation is *trnQ–atp6–nad1–cob–trnF–cox1–trnI* (Figure 12A). Since the obtained sequence is incomplete and several regions remain unannotated, this configuration should be viewed solely as the local gene order of the assembled fragment, rather than the complete mitochondrial gene order of *B. valkanovi*. No ribosomal RNA gene was confidently identified.

The four (PCGs) displayed continuous open reading frames (ORFs) when considering the mitochondrial genetic code of echinoderms and flatworms. The *atp6* and *nad1* genes started with the codon ATG, while the *cob* gene began with ATC. All three genes ended with the stop codon TAA. The *cox1* sequence, which measures 1572 bp, translated into a continuous protein consisting of 523 amino acids and was marked by an inferred non-canonical initiation codon TTG and a termination codon TAG. Paired-read mapping

provided evidence of sequence continuity across the initial assembly boundary that this gene crosses.

Manual annotation and validation: The manual curation process significantly reduced the number of features initially identified through automatic annotation. The boundaries of the four retained PCGs were confirmed by the absence of internal stop codons and by comparative protein analysis. The expected products varied in size, starting from 227 amino acids in *atp6* to 523 amino acids in *cox1*.

Three tRNA genes, 67–71 bp long, were retained after independent sequence- and structure-based validation. The 71-bp *trnI* contained the GAT anticodon and produced a complete cloverleaf-compatible secondary structure. The 70-bp *trnF* contained the GAA anticodon, whereas the 67-bp *trnQ* contained the TTG anticodon (Figure 12(B1,B2)). For all three genes, the MiTFi predictions were supported by tRNAscan-SE, Q-INS-i comparative alignments and manual inspection of the predicted secondary structures. Two identical *trnQ* (TTG) candidates were initially detected in repeated regions of the assembly. Paired-read mapping supported both external junctions of the retained candidate. In contrast, one junction of the alternative candidate was contradicted by a recurrent high-mapping-quality gapped alignment, whereas reads matching the assembled junction were sparse and ambiguously placed. The latter candidate was consequently interpreted as a repeat-associated assembly artefact and excluded, and only one *trnQ* copy was retained (Figure 12(B1,B2)). Other unresolved tRNA predictions were likewise excluded from the validated gene set.

5. Discussion

5.1. Morphological Discussion of the New Species

The habitus and internal organisation of species of *Baltoplana*, including the female reproductive system, are highly similar and do not offer notable diagnostic characters to differentiate among species. However, the male reproductive system shows notable variation and serves as a sound base for species identification (Table 4) [13,15,16,18]. The most important distinguishing feature of the male reproductive system is whether the ejaculatory duct is unarmed (only in *B. bisphaera* Jouk & De Vocht, 1989) or forms an armed cirrus. Also, the presence and number of accessory cirri (absent in *B. pseudovalkanovi* n. sp., *B. brusai* n. sp., and *B. valkanovi*) is a useful character, which can easily be observed even in live animals. In species that have a cirrus and accessory cirri, the size and shape of the spines are also important characters for identification. The presence of sclerotised tissue in the distal region of the copulatory bulb, which can form a cap, a ring or none of these structures, is also relevant. The cirrus' armature consists of sclerotised ridges (as seen on histological sections) that project towards the lumen and are distinguished as spines in live specimens and whole mounts ([13] and our own observations).

To facilitate species comparison, we organised species of *Baltoplana* in three groups based on the morphology of the copulatory bulb: **(1)** species with an unsclerotised ejaculatory duct, i.e., a cirrus is not present; **(2)** species with a cirrus but lacking a distal cap; and **(3)** species with a cirrus and a distal cap or ring. Species with accessory cirri can occur in all of the three groups.

An unsclerotised (unarmed) ejaculatory duct is only present in *B. bisphaera*, which is also characterised by the presence of two-armed accessory cirri [16]. All other species of *Baltoplana* have a sclerotised, spiny region of the ejaculatory duct that forms a cirrus.

In the second group of species, some sclerotised tissue may accompany the cirrus in the distal part of the copulatory bulb, but it is not organised to form a cap or a ring. The copulatory bulb in this group may or may not have accessory cirri. These species include *B. bipartita* n. sp., *B. cupressus*, *B. magna*, *B. pseudovalkanovi* n. sp., *B. quadricirrata* n. sp., *B. tricirrata* n. sp., and *B. valkanovi*. These species are primarily differentiated by the

presence and number of accessory cirri: accessory cirri are lacking in *B. valkanovi* and *B. pseudovalkanovi* n. sp., one accessory cirrus occurs in *B. cupressus* and *B. bipartita* n. sp., two in *B. magna*, three in *B. tricirrata* n. sp., and four in *B. quadricirrata* n. sp.

Baltoplana pseudovalkanovi n. sp. and *B. valkanovi* are similar in morphology but differ from each other due to the much shorter and wider cirrus in the former (144 × 20 µm vs. 216 × 6 µm, respectively) ([15] and this study). The distribution and size of the spines also differ between these two species: in *B. pseudovalkanovi* n. sp., the spines are longer in the cirrus's proximal region (12 µm) and decrease in size towards the distal region (6 µm long). In contrast, the cirrus of *B. valkanovi* shows three spiny regions, with spines measuring ~1–2 µm proximally, increasing to ~7 µm in the middle region, and slightly decreasing to ~5 µm distally. Additionally, *B. pseudovalkanovi* n. sp. and *B. valkanovi* exhibit a disjunct distribution, being found in the Southwestern Atlantic and the Black Sea, respectively, suggesting that both species are geographically isolated.

Baltoplana cupressus and *B. bipartita* n. sp. both have a single accessory cirrus; however, they differ in their structure and ornamentation. In *B. cupressus*, both the cirrus and accessory cirrus measure approximately 23 µm, and the hooks of the proboscis bear small denticles [18], a feature only observed in *B. brusai* n. sp. In contrast, *B. bipartita* n. sp. is characterised by a conspicuous 143-µm-long cirrus with robust, and elongated spines (44 µm proximally and 22 µm distally) and a 124-µm-long accessory cirrus with very long spines (up to 72 µm). This organisation is unique within *Baltoplana* and clearly distinguishes *B. bipartita* n. sp. from *B. cupressus*, as well as from other congeners.

In addition to the differences in the number of accessory cirri, *B. magna*, *B. tricirrata* n. sp., and *B. quadricirrata* n. sp. can also be differentiated by the length of the cirrus: 216 µm, 208 µm, and 93 µm, respectively. Furthermore, the shape, distribution and size of the spines along the cirri vary: *B. magna* has longer spines (13 µm proximally and 3 µm distally), in *B. tricirrata* n. sp. the spines increase in length from the proximal (1–3 µm) to the distal end (up to 8 µm), and in *B. quadricirrata* n. sp. all the spines are ca. 7 µm. Moreover, the accessory cirri in *B. magna* are spherical and similar in length (65 µm long), and each bears large spines measuring 18 µm. In contrast, *B. tricirrata* n. sp. and *B. quadricirrata* n. sp. have shorter accessory cirri that vary in length and shape. Specifically, the lengths of the accessory cirri for *B. tricirrata* n. sp. are 44 µm, 28 µm, and 83 µm, while the lengths for *B. quadricirrata* n. sp. are 45 µm, 37 µm, 34 µm, and 26 µm. Furthermore, the spines on the accessory cirri of the latter two species are shorter (7–10 µm long and 4–14 µm long, respectively) than those of *B. magna* [13].

Finally, the third group of species includes those with a cirrus and a distal cap or ring: *B. floridana* n. sp., *B. galerita* n. sp., and *B. brusai* n. sp. Among these, *B. floridana* n. sp. is unique because the sclerotised tissue forms a subterminal ring surrounding the ejaculatory duct and does not form a cap as in the other two species. *Baltoplana floridana* n. sp. is also unique since the ejaculatory duct proximally shows three coils and the proximal part of the cirrus exhibits zig-zag-shaped striation. Moreover, the two accessory cirri measure 11 µm in length. The cirrus of the two other species, *B. galerita* n. sp. and *B. brusai* n. sp., lacks sclerotised striations. *B. galerita* n. sp. shows a proximal coil in the ejaculatory duct, which is not the case in *B. brusai* n. sp. *Baltoplana galerita* n. sp. has a 128-µm-long cirrus and a 23-µm-long single accessory cirrus, whereas *B. brusai* n. sp. has a shorter, 70-µm-long cirrus with no accessory cirri. In addition, *B. brusai* n. sp. presents cirrus spines that are longer in the proximal and middle regions (9 µm long) and gradually become shorter in the distal region (5 µm long), whereas cirrus spines in *B. galerita* n. sp. vary from 5 to 12 µm, but are almost of the same size distally (8 µm long). Another difference between *B. galerita* n. sp. and *B. brusai* n. sp. is the ratio of the cap/cirrus length (~11% vs. ~18%, respectively). Moreover, *B. galerita* n. sp. can further be distinguished from *B. brusai* n. sp. because the

latter species exhibits a denticle on the internal side of each proboscis hook, which is not present in *B. galerita* n. sp.

5.2. Identification Key

The previous discussion on the genus *Baltoplana* is summarised in the following identification key.

1a. Ejaculatory duct unarmed, without a spiny cirrus; two spherical accessory cirri .....*B. bisphaera*.

1b. Ejaculatory duct forming a spiny, sclerotised cirrus .....2.

2a. Accessory cirri absent.....3.

2b. One or more accessory cirri present .....5.

3a. Proboscis hooks each with one denticle on the inner side; distal end of the copulatory bulb with a sclerotised cap (12 × 16 µm) .....*B. brusai* n. sp.

3b. Proboscis hooks smooth; copulatory bulb without a cap.....4.

4a. Cirrus stout, 12–29 µm wide; cirrus spines longest proximally (mean 12 µm) and shortest distally (mean 6 µm) .....*B. pseudovalkanovi* n. sp.

4b. Cirrus slender, 5–9 µm wide; cirrus spines shortest proximally (1–2 µm) and longest in the middle region (mean 7 µm) .....*B. valkanovi*.

5a. One accessory cirrus.....6.

5b. Two or more accessory cirri.....8.

6a. Distal end of the copulatory bulb with a sclerotised cap (14 × 38 µm, ca. 11% of the cirrus length) .....*B. galerita* n. sp.

6b. Copulatory bulb without a distal cap.....7.

7a. Proboscis hooks each with one denticle on the inner side; cirrus short and stout, 23 µm long and 18 µm wide (length:width ca. 1.3); accessory cirrus 23 µm long, elongate.....*B. cupressus*.

7b. Proboscis hooks smooth; cirrus 143 µm long, with robust spines (44 µm proximally, 22 µm distally); accessory cirrus 124 µm long, bipartite, with spines up to 72 µm .....*B. bipartita* n. sp.

8a. Two accessory cirri.....9.

8b. Three or four accessory cirri.....10.

9a. Copulatory bulb with a subterminal sclerotised ring 21 µm wide; proximal half of the cirrus with zigzag sclerotised ridges and spines restricted to the distal half; accessory cirri 11 µm long.....*B. floridana* n. sp.

9b. Copulatory bulb without a sclerotised ring; cirrus spiny along its whole length; accessory cirri spherical, 65 µm long, with 18-µm spines.....*B. magna*.

10a. Three accessory cirri of unequal length (83, 44 and 28 µm); cirrus spines increasing in length from proximal (2 µm) to distal (8 µm) .....*B. tricirrata* n. sp.

10b. Four accessory cirri (45, 37, 34 and 26 µm); cirrus spines of ± uniform length (ca. 7 µm) .....*B. quadricirrata* n. sp.

5.3. Phylogenetic Relationships

Our phylogenetic results are identical to those of previous studies in recovering Cheliplanidae as monophyletic (i.e., [6–8,61]), along with two other groups (both species of *Carcharodorhynchus* and all other schizorhynchids) within Schizorhynchia (i.e., [8]). However, here we provide a thorough analysis of the internal relationships of Cheliplanidae with five times more sequenced specimens of the family. These data include the first sequences of representatives of *Baltoplana* (two species) and of six species of *Cheliplana*.

The monophyly of Cheliplanidae is also supported by the morphological similarities among species of the genera it contains (*Baltoplana*, *Cheliplana*, *Cheliplanilla*,

Archipelagoplana, and *Freddius*). These similarities include the overall habitus, a barrel-shaped, horizontally oriented pharynx, the presence of an armed proboscis, and the conjuncta-duplex–type copulatory bulb, mostly presenting some degrees of sclerotisation and/or ornamentation [13,19,62,63].

In contrast, current analyses highlight the contradictions between morphology-diagnosed genera and phylogenetic results, as the sampled representatives of *Baltoplana* do not form a monophyletic group. The analyses of both the combined (18S and 28S), as well as the 18S-only dataset, strongly rejected the hypothesis that the two sampled species of *Baltoplana* form a monophyletic group. This rejection was consistently supported by various topology tests (KH, SH, and AU), suggesting that the restricted topology that assumes the monophyly of *Baltoplana* does not adequately align with the molecular data. It must be stressed, however, that this result rests on a very sparse sample of the genus: molecular data are available for only two of the eleven species now assigned to *Baltoplana* (*B. magna* and *B. galerita* n. sp.), so that nine species, including six of the seven described here, are not represented in the analyses. What the topology tests demonstrate is, therefore, an incompatibility between the current circumscription of the genus and the topology recovered from the sampled taxa, rather than polyphyly of *Baltoplana* as a whole. One possible explanation for this result is the missing data in the concatenated analysis, as *B. magna* is represented only by an 18S sequence, while for the one specimen of *B. galerita* n. sp. both 18S and 28S data are available, and the second specimen is represented by 18S only. It has been suggested that missing-data sequences can impact phylogenetic inference [64]. Nevertheless, this scenario is unlikely to account for the current results, since the analysis using the 18S marker alone—where direct comparison between both species of *Baltoplana* is possible—led to identical results. This suggests that the recovered phylogenetic relationship is highly influenced by the signal of the 18S gene and cannot be solely explained by the lack of 28S data for *Baltoplana*. We stress, however, that the scope of this comparison is limited. It excludes the possibility that the result is an artefact of the empty 28S cells, but it does not establish that the relationship is robust to the choice of marker, since the same 18S signal dominates both analyses and the two genes are not independent of one another (see below). A conclusive test would require unlinked nuclear loci or genome-scale data. The situation of *Cheliplana* is different. The sampled species of *Cheliplana* do form a clade in all unconstrained analyses—in the concatenated 18S–28S dataset, in the 18S-only dataset and in the Bayesian consensus—but the node subtending them falls below the support thresholds applied in Figure 11 (SH-aLRT 7.6/UFboot 56 and pp 0.80 in the concatenated analyses, UFboot 85 in the 18S-only analysis) and is therefore collapsed there. What Figure 11 shows for *Cheliplana* is thus a lack of resolution, not a contradiction of the genus as currently circumscribed. The topology tests point in the same direction: enforcing the monophyly of *Cheliplana* returned a tree essentially indistinguishable from the unconstrained one in both datasets (ΔLogL = 0.0004 and 0.0003, respectively), and none of the KH, SH or AU tests rejected the constrained hypothesis ($p \geq 0.476$ throughout; Table 5). The present data therefore neither corroborate nor reject the monophyly of *Cheliplana* with confidence: they simply do not resolve it. Broader sampling of the taxa involved and the incorporation of independent, unlinked molecular markers are, therefore, necessary to establish whether the incompatibility recovered here among the sampled species of *Baltoplana* extends to the genus as a whole, and to test the monophyly of *Cheliplana*, which the present data do not resolve. Such a broader analysis is especially warranted because the general anatomy of species of *Baltoplana* is very homogeneous and they are easily differentiable from all other cheliplanids by the presence of two ovaries, paired sclerotised bursal nozzles, and insemination ducts [13,15,16,18], a characteristic only shown by the unrelated species of *Carcharodorhynchus*. In addition, species of *Cheliplanilla* are unique due to the presence of

paired denticles on the proboscis hook and cuticular proboscis' side pieces with crossbar, and one of the seminal vesicles is blind [62,63,65]. Species of *Cheliplana*, otherwise, exhibit more morphological variability, particularly of the genital systems. However, all of them present a single ovary and the proboscis side pieces are mostly not sclerotised, and when sclerotised lack the crossbar [22]. Because of the morphological uniformity within each of the three genera *Baltoplana*, *Cheliplana* and *Cheliplanilla*—whose species differ from one another essentially only in the genital system, and in *Baltoplana* almost exclusively in the male copulatory organ (Table 4)—and because taxon sampling is still limited, we refrain from implementing any taxonomic changes. Furthermore, we must keep in mind that the 18S and 28S markers, broadly used to infer phylogenetic relationships within Platyhelminthes and Rhabdocoela, may not be equally informative within Cheliplanidae. Both genes belong to the same ribosomal cistron and are, therefore, physically linked, so that concatenating them does not provide independent lines of evidence, and both are conserved enough that the short internal branches separating the genera of the family may fall below their resolving power. As noted above, testing the generic limits within Cheliplanidae will, therefore, require markers that are genuinely independent of one another: several unlinked nuclear loci, or genome-scale datasets such as those obtained by target enrichment or from transcriptomes. A distinct question, better suited to faster-evolving markers, is the delimitation of species within each genus, for which *cox1* and ITS are appropriate and would allow the morphologically defined species boundaries proposed here to be tested. The annotated partial mitochondrial genome of *B. valkanovi* reported here contributes to the latter aim rather than the former, providing the first mitochondrial reference for the genus (see Section 5.4).

Another valid alternative explanation is that previously recognised apomorphies of the analysed genera have evolved independently several times, such as the number of ovaries and the structure of the proboscis. If further phylogenetic studies confirm the non-monophyly of *Baltoplana*, and if broader sampling should also reject the monophyly of *Cheliplana*, ideally including data from the still unsequenced genera *Freddius* and *Archipelagoplana*, a deeper morphological account will be needed to identify additional diagnostic characters for the resulting clusters.

5.4. Mitochondrial Genome of Baltoplana valkanovi

The partial mitochondrial genome of *B. valkanovi*, which spans 7154 bp, serves as the initial mitogenomic reference for this species and adds a free-living schizorhynchian lineage to the currently uneven representation of Rhabdocoela. This fragment is rich in adenine and thymine (65.9%) and comprises four annotated protein-coding genes—*atp6*, *nad1*, *cob* (*cytb*), and *cox1*—as well as three mitochondrial tRNAs—*trnQ*, *trnF*, and *trnI*. All are encoded on the same strand, which aligns with the mostly unidirectional transcription observed in flatworm mitochondrial genomes [11,66]. Since only part of the genome was recovered, this arrangement cannot be extrapolated to the complete mitogenome. The four protein-coding sequences form uninterrupted ORFs under the echinoderm and flatworm mitochondrial genetic code [67]. Unlike the abbreviated termination codons commonly reported in rhabdocoels and other metazoan mitogenomes [11,12,68], all four genes in *B. valkanovi* terminate with complete TAA or TAG codons. *atp6* and *nad1* initiate with ATG, whereas *cob* uses ATC and the beginning of *cox1* was inferred to use TTG. Alternative mitochondrial start codons have been reported in flatworms [10,69], but the TTG boundary of *cox1* remains unusual and should be interpreted as a comparative annotation supported by an uninterrupted ORF and read continuity rather than direct evidence of translation initiation. Importantly, reads spanning the original assembly boundary support the local continuity of *cox1*, but do not establish circularity of the mitochondrial chromosome.

The four annotated protein-coding genes sample four complexes of the oxidative phosphorylation pathway and broaden the molecular record beyond *cox1*, the widely used animal DNA barcode, for which universal primers often perform poorly in molecularly divergent flatworm lineages [70]. The sequences reported here can therefore support the design of lineage-specific primers and provide additional mitochondrial markers for future work within *Baltoplana*, Cheliplanidae and Schizorhynchia.

No *atp8* sequence could be annotated confidently. This gene is short and exceptionally divergent in turbellarian flatworms, making its detection strongly dependent on manual curation and, ideally, transcriptomic or proteomic evidence [10,71,72]. Monnens et al. [11,12] similarly refrained from equating failure to annotate *atp8* with gene loss when the available genomic evidence was inconclusive. This distinction is particularly important here because the assembly is incomplete: *atp8* may occur outside the recovered fragment or be present as a highly divergent ORF that cannot be reliably identified from genomic sequence alone. Moreover, the extensive mitochondrial rearrangements documented among rhabdocoels mean that *atp8* presence cannot be inferred exclusively from the region adjacent to *atp6*. Accordingly, the appropriate conclusion is that *atp8* was not recovered or confidently annotated, rather than that it is absent.

The retained tRNAs range from 67 to 71 bp and possess the expected anticodons for glutamine, phenylalanine, and isoleucine. *trnF*(GAA) produced the strongest and most conventional cloverleaf prediction, while *trnI*(GAU) showed a plausible cloverleaf-compatible structure. *trnQ*(UUG) received a lower prediction score and exhibited a reduced T arm, but its anticodon, comparative alignment, structural model, and read support collectively justified its conservative retention. These differences illustrate why mitochondrial tRNAs should not be accepted or rejected solely on the output of a single prediction program [11]. Duplications and transpositions of mitochondrial tRNA genes are known to occur among rhabdocoels [12]. Although preliminary analyses of *B. valkanovi* also produced additional or duplicate-like tRNA predictions, only one copy each of *trnQ*, *trnF*, and *trnI* satisfied the combined annotation criteria. The excluded predictions should, therefore, not be treated as evidence of genuine tRNA duplication or loss.

Finally, the local succession of the validated genes demonstrates that the fragment contains potentially informative architectural characters. Gene order varies considerably among the rhabdocoel mitogenomes sequenced so far [11,12], which reinforces earlier warnings that this character is phylogenetically informative only under dense taxon sampling [73]. In *B. valkanovi*, unrecovered genes and long unannotated intervals prevent reconstruction of the complete gene order. The principal contribution of this partial mitogenome is therefore a validated reference fragment—homologous coding sequences, tRNA identities and anticodons, and their local associations—for a free-living schizorhynch lineage for which no mitogenomic data previously existed. Completing the mitogenome with complementary sequencing data will be necessary to evaluate its full gene complement, confirm chromosome structure, and determine whether its architecture contains rearrangements characteristic of *Baltoplana* or Schizorhynchia.

Supplementary Materials: The following supporting information can be downloaded at https://www.mdpi.com/article/10.3390/d18110650/s1, Figure S1: Uncollapsed maximum-likelihood tree of the concatenated 18S + 28S rDNA alignment, with SH-aLRT and ultrafast bootstrap support at every node; Figure S2: Uncollapsed Bayesian majority-rule consensus tree of the concatenated 18S + 28S rDNA alignment, with posterior probabilities at every node; Figure S3: Uncollapsed maximum-likelihood tree of the 18S rDNA alignment, with ultrafast bootstrap support at every node; File S1: IQ-TREE command lines and MrBayes block as executed.

Author Contributions: Conceptualisation, J.R., M.M. and T.A.; methodology, J.R., L.V., Y.L.D., M.M. and T.A.; formal analysis, J.R., Y.L.D., M.M., L.V. and T.A.; resources, P.E.H.J., N.J.P.R., E.S., P.R., Y.L.D.,

M.M. and T.A.; writing—original draft preparation, J.R., Y.L.D. and M.M.; writing—review and editing, M.M. and T.A.; funding acquisition, T.A. All authors have read and agreed to the published version of the manuscript.

Funding: This study was supported by the Special Research Fund (BOF), Hasselt University: R-15182/BOF24OWB13. YLD is supported by the Smithsonian Institution through the SMS Post-doctoral Fellowship Program, which is partially funded by the Link Foundation. This is Smithsonian Marine Station contribution No. 1264. The research leading to the results presented in this publication was partially carried out with infrastructure funded by EMBRC Belgium-FWO project GOH3817N.

Data Availability Statement: The original data presented in the study are openly available in GenBank, in the NCBI Sequence Read Archive and in Zenodo. The newly generated 18S and 28S rRNA gene sequences are available in GenBank under the accession numbers listed in Table 2. The partial mitochondrial contig of *Baltoplana valkanovi* is available in GenBank under accession number PZ818244 (Table 6). The raw sequencing reads are available from the NCBI Sequence Read Archive under BioProject accession number PRJNA1533030. The sequence alignments, the phylogenetic trees with all support values, the software configuration files and the complete output of the partition-sensitivity analysis are openly available in Zenodo at https://doi.org/10.5281/zenodo.22917871.

Acknowledgments: N. Steffanie is thanked for producing the sectioned material, and Ria Vanderspikken for her invaluable administrative support in the laboratory. Alexander Parry is thanked for providing the sediment samples from Palm Beach, Florida. Marco Curini-Galletti kindly hosted YLD during the collection in Tuscany. Collecting permission in Florida was covered by the Special Activity License SAL-24-2639B-SR issued by the Florida Fish and Wildlife Conservation Commission to Holly Sweat.

Conflicts of Interest: The authors declare no conflicts of interest.

References

1. Balsamo, M.; Artois, T.; Smith, J.P.S.; Todaro, M.A.; Guidi, L.; Leander, B.S.; Van Steenkiste, N.W.L. The curious and neglected soft-bodied meiofauna: Rouphozoa (Gastrotricha and Platyhelminthes). *Hydrobiologia* **2020**, *847*, 2613–2644. [CrossRef] [PubMed]
2. Aramayo, V. Diversidad, densidad y distribución vertical de la meiofauna bentónica en sedimentos fangosos frente a Perú central (12° S). *Bol. Inst. Mar. Perú* **2018**, *33*, 90–97.
3. Schratzberger, M.; Ingels, J. Meiofauna matters: The roles of meiofauna in benthic ecosystems. *J. Exp. Mar. Biol. Ecol.* **2018**, *502*, 12–25. [CrossRef]
4. Martínez, A.; Fontaneto, D.; Curini-Galletti, M. The swash zone selects functionally specialized assemblages of beach interstitial meiofauna (Platyhelminthes, Proseriata). *Ecography* **2024**, *4*, 527–534. [CrossRef]
5. Tyler, S.; Artois, T.; Schilling, S.; Hooge, M.; Bush, L.F. (Eds.) World List of Turbellarian Worms: Acoelomorpha, Catenulida, Rhabditophora. Schizorhynchia. 2006–2026. Available online: https://www.marinespecies.org/aphia.php?p=taxdetails&id=155663 (accessed on 14 September 2026).
6. Tessens, B.; Janssen, T.; Artois, T. Molecular phylogeny of Kalyptorhynchia (Rhabdocoela, Platyhelminthes) inferred from ribosomal sequence data. *Zool. Scr.* **2014**, *43*, 519–530. [CrossRef]
7. Smith, J.P.S., III; Litvaitis, M.K.; Gobert, S.; Uyeno, T.; Artois, T. Evolution and functional morphology of the proboscis in Kalyptorhynchia (Platyhelminthes). *Integr. Comp. Biol.* **2015**, *55*, 205–216. [CrossRef] [PubMed]
8. Diez, Y.L.; Reyes, J.; Hermans, S.; Sweat, L.H.; Monnens, M.; Artois, T. Phylogenetic relationships of a new schizorhynch genus refute the monophyly of *Schizochilus* Boaden, 1963 (Platyhelminthes, Rhabdocoela). *Mar. Biodivers.* **2026**, *56*, 26. [CrossRef]
9. Gissi, C.; Iannelli, F.; Pesole, G. Evolution of the mitochondrial genome of Metazoa as exemplified by comparison of congeneric species. *Heredity* **2008**, *101*, 301–320. [CrossRef] [PubMed]
10. Ross, E.; Blair, D.; Guerrero-Hernández, C.; Sánchez Alvarado, A. Comparative and transcriptome analyses uncover key aspects of coding- and long noncoding RNAs in flatworm mitochondrial genomes. *G3 Genes Genomes Genet.* **2016**, *6*, 1191–1200. [CrossRef] [PubMed]
11. Monnens, M.; Thijs, S.; Briscoe, A.G.; Clark, M.; Frost, E.J.; Littlewood, D.T.J.; Sewell, M.; Smeets, K.; Artois, T.; Vanhove, M.P.M. The first mitochondrial genomes of endosymbiotic rhabdocoels illustrate evolutionary relaxation of *atp8* and genome plasticity in flatworms. *Int. J. Biol. Macromol.* **2020**, *162*, 454–469. [CrossRef] [PubMed]
12. Monnens, M.; Artois, T.; Briscoe, A.; Diez, Y.L.; Fraser, K.P.P.; Leander, B.S.; Littlewood, D.T.J.; Santos, M.J.; Smeets, K.; Van Steenkiste, N.W.L.; et al. Signatures of endosymbiosis in mitochondrial genomes of rhabdocoel flatworms. *Mol. Ecol.* **2025**, *34*, e70015. [CrossRef] [PubMed]

13. Karling, T.G. Studien über Kalyptorhynchien (Turbellaria). II. Die Familien Karkinorhynchidae und Diascorhynchidae. *Acta Zool. Fenn.* **1949**, *58*, 1–42.
14. Karling, T.G. Turbellarian fauna of the Baltic proper: Identification, ecology and biogeography. *Fauna Fenn.* **1974**, *27*, 1–101.
15. Ax, P. Zur Systematik, Ökologie und Tiergeographie der Turbellarienfauna in den ponto-kaspischen Brackwassermeeren. *Zool. Jahrb. Abt. Syst. Ökol. Geogr. Tiere* **1959**, *87*, 43–187.
16. Jouk, P.E.H.; De Vocht, A.J.P. Kalyptorhynchia (Plathelminthes Rhabdocoela) from the Kenyan coast, with descriptions of four new species. *Trop. Zool.* **1989**, *2*, 145–157. [CrossRef]
17. Noreña, C.; Damborenea, C.; Faubel, A.; Brusa, F. Composition of meiobenthonic Platyhelminthes from brackish environments of the Galician and Cantabrian coasts of Spain with the description of a new species of *Djeziraia* (Polycystididae, Kalyptorhynchia). *J. Nat. Hist.* **2007**, *41*, 1989–2005. [CrossRef]
18. Willems, W.R.; Reygel, P.; Van Steenkiste, N.; Tessens, B.; Artois, T.J. Kalyptorhynchia (Platyhelminthes: Rhabdocoela) from KwaZulu-Natal (South Africa), with the description of six new species. *Zootaxa* **2017**, *4242*, 441–466. [CrossRef] [PubMed]
19. Karling, T.G. Morphologisch-histologische Untersuchungen an den männlichen Atrialorganen der Kalyptorhynchia (Turbellaria). *Ark. Zool.* **1956**, *9*, 187–277.
20. Martens, P.M. Comparison of three different extraction methods for Turbellaria. *Mar. Ecol. Prog. Ser.* **1984**, *14*, 229–234. [CrossRef]
21. Schockaert, E.R. The importance of turbellarians in ecosystems. In *Methods for the Examination of Organismal Diversity in Soils and Sediments*; Hall, G.S., Ed.; CAB International: Wallingford, UK, 1996; pp. 211–225.
22. Gobert, S.; Diez, Y.L.; Monnens, M.; Reygel, P.; Van Steenkiste, N.W.L.; Leander, B.S.; Artois, T. A revision of the genus *Cheliplana* de Beauchamp, 1927 (Rhabdocoela: Schizorhynchia), with the description of six new species. *Zootaxa* **2021**, *4970*, 453–494. [CrossRef] [PubMed]
23. Cracraft, J. Species concepts and speciation analysis. In *Current Ornithology*; Johnston, R.F., Ed.; Plenum Press: New York, NY, USA, 1983; Volume 1, pp. 159–187. [CrossRef]
24. Wheeler, Q.D.; Platnick, N.I. The phylogenetic species concept (sensu Wheeler and Platnick). In *Species Concepts and Phylogenetic Theory: A Debate*; Wheeler, Q.D., Meier, R., Eds.; Columbia University Press: New York, NY, USA, 2000; pp. 55–69.
25. International Commission on Zoological Nomenclature. *International Code of Zoological Nomenclature*, 4th ed.; International Trust for Zoological Nomenclature: London, UK, 1999. Available online: https://code.iczn.org/ (accessed on 15 December 2025).
26. Laumer, C. Picogram Input Multimodal Sequencing (PiMmS). 2023. Available online: https://www.protocols.io/view/picogram-input-multimodal-sequencing-pimms-rm7vzywy5lx1/v1 (accessed on 12 November 2025).
27. Kearse, M.; Moir, R.; Wilson, A.; Stones-Havas, S.; Cheung, M.; Sturrock, S.; Buxton, S.; Cooper, A.; Markowitz, S.; Duran, C.; et al. Geneious Basic: An integrated and extendable desktop software platform for the organisation and analysis of sequence data. *Bioinformatics* **2012**, *28*, 1647–1649. [CrossRef] [PubMed]
28. Altschul, S.F.; Gish, W.; Miller, W.; Myers, E.W.; Lipman, D.J. Basic local alignment search tool. *J. Mol. Biol.* **1990**, *215*, 403–410. [CrossRef] [PubMed]
29. Benson, D.A.; Karsch-Mizrachi, I.; Clark, K.; Lipman, D.J.; Ostell, J.; Sayers, E.W. GenBank. *Nucleic Acids Res.* **2012**, *40*, D48–D53. [CrossRef] [PubMed]
30. Norén, M.; Jondelius, U. Phylogeny of the Prolecithophora (Platyhelminthes) inferred from 18S rDNA sequences. *Cladistics* **1999**, *15*, 103–112. [CrossRef] [PubMed]
31. Littlewood, D.T.J.; Curini-Galletti, M.; Herniou, E.A. The interrelationships of Proseriata (Platyhelminthes: Seriata) tested with molecules and morphology. *Mol. Phylogenet. Evol.* **2000**, *16*, 449–466. [CrossRef]
32. Katoh, K.; Standley, D.M. MAFFT multiple sequence alignment software version 7: Improvements in performance and usability. *Mol. Biol. Evol.* **2013**, *30*, 772–780. [CrossRef] [PubMed]
33. Katoh, K.; Rozewicki, J.; Yamada, K.D. MAFFT online service: Multiple sequence alignment, interactive sequence choice and visualization. *Brief. Bioinform.* **2017**, *20*, 1160–1166. [CrossRef] [PubMed]
34. Kalyaanamoorthy, S.; Minh, B.Q.; Wong, T.K.F.; von Haeseler, A.; Jermiin, L.S. ModelFinder: Fast model selection for accurate phylogenetic estimates. *Nat. Methods* **2017**, *14*, 587–589. [CrossRef] [PubMed]
35. Wong, T.K.F.; Ly-Trong, N.; Ren, H.; Baños, H.; Roger, A.J.; Susko, E.; Bielow, C.; De Maio, N.; Goldman, N.; Hahn, M.W.; et al. IQ-TREE 3: Phylogenomic inference software using complex evolutionary models. *Mol. Biol. Evol.* **2026**, *43*, msag117. [CrossRef] [PubMed]
36. Kainer, D.; Lanfear, R. The effects of partitioning on phylogenetic inference. *Mol. Biol. Evol.* **2015**, *32*, 1611–1627. [CrossRef]
37. Nguyen, L.-T.; Schmidt, H.A.; von Haeseler, A.; Minh, B.Q. IQ-TREE: A fast and effective stochastic algorithm for estimating maximum-likelihood phylogenies. *Mol. Biol. Evol.* **2015**, *32*, 268–274. [CrossRef] [PubMed]
38. Hoang, D.T.; Chernomor, O.; von Haeseler, A.; Minh, B.Q.; Vinh, L.S. UFBoot2: Improving the ultrafast bootstrap approximation. *Mol. Biol. Evol.* **2018**, *35*, 518–522. [CrossRef] [PubMed]
39. Guindon, S.; Dufayard, J.-F.; Lefort, V.; Anisimova, M.; Hordijk, W.; Gascuel, O. New algorithms and methods to estimate maximum-likelihood phylogenies: Assessing the performance of PhyML 3.0. *Syst. Biol.* **2010**, *59*, 307–321. [CrossRef] [PubMed]

40. Ronquist, F.; Teslenko, M.; van der Mark, P.; Ayres, D.L.; Darling, A.; Höhna, S.; Larget, B.; Liu, L.; Suchard, M.A.; Huelsenbeck, J.P. MrBayes 3.2: Efficient Bayesian phylogenetic inference and model choice across a large model space. *Syst. Biol.* **2012**, *61*, 539–542. [CrossRef] [PubMed]
41. Rambaut, A. FigTree: Tree Figure Drawing Tool, Version 1.4.4. 2006–2019. Available online: http://tree.bio.ed.ac.uk/software/figtree/ (accessed on 15 January 2026).
42. Kishino, H.; Hasegawa, M. Evaluation of the maximum likelihood estimate of the evolutionary tree topologies from DNA sequence data, and the branching order in Hominoidea. *J. Mol. Evol.* **1989**, *29*, 170–179. [CrossRef] [PubMed]
43. Shimodaira, H.; Hasegawa, M. Multiple comparisons of log-likelihoods with applications to phylogenetic inference. *Mol. Biol. Evol.* **1999**, *16*, 1114–1116. [CrossRef]
44. Shimodaira, H. An approximately unbiased test of phylogenetic tree selection. *Syst. Biol.* **2002**, *51*, 492–508. [CrossRef] [PubMed]
45. Dierckxsens, N.; Mardulyn, P.; Smits, G. NOVOPlasty: De novo assembly of organelle genomes from whole genome data. *Nucleic Acids Res.* **2017**, *45*, e18. [CrossRef] [PubMed]
46. Andrews, S. FastQC: A Quality Control Tool for High Throughput Sequence Data. Babraham Bioinformatics: Cambridge, UK, 2010. Available online: https://www.bioinformatics.babraham.ac.uk/projects/fastqc/ (accessed on 15 December 2025).
47. Jalili, V.; Afgan, E.; Gu, Q.; Clements, D.; Blankenberg, D.; Goecks, J.; Taylor, J.; Nekrutenko, A. The Galaxy platform for accessible, reproducible and collaborative biomedical analyses: 2020 update. *Nucleic Acids Res.* **2020**, *48*, W395–W402, Correction in *Nucleic Acids Res.* **2020**, *48*, 8205–8207. https://doi.org/10.1093/nar/gkaa554. [CrossRef] [PubMed]
48. Bernt, M.; Donath, A.; Jühling, F.; Externbrink, F.; Florentz, C.; Fritzsch, G.; Pütz, J.; Middendorf, M.; Stadler, P.F. MITOS: Improved de novo metazoan mitochondrial genome annotation. *Mol. Phylogenet. Evol.* **2013**, *69*, 313–319. [CrossRef] [PubMed]
49. Donath, A.; Jühling, F.; Al-Arab, M.; Bernhart, S.H.; Reinhardt, F.; Stadler, P.F.; Middendorf, M.; Bernt, M. Improved annotation of protein-coding genes boundaries in metazoan mitochondrial genomes. *Nucleic Acids Res.* **2019**, *47*, 10543–10552. [CrossRef] [PubMed]
50. Edgar, R.C. Muscle5: High-accuracy alignment ensembles enable unbiased assessments of sequence homology and phylogeny. *Nat. Commun.* **2022**, *13*, 6968. [CrossRef] [PubMed]
51. Camacho, C.; Coulouris, G.; Avagyan, V.; Ma, N.; Papadopoulos, J.; Bealer, K.; Madden, T.L. BLAST+: Architecture and applications. *BMC Bioinform.* **2009**, *10*, 421. [CrossRef] [PubMed]
52. Kenny, N.J.; Noreña, C.; Damborenea, C.; Grande, C. Probing recalcitrant problems in polyclad evolution and systematics with novel mitochondrial genome resources. *Genomics* **2019**, *111*, 343–355. [CrossRef] [PubMed]
53. Lowe, T.M.; Chan, P.P. tRNAscan-SE On-line: Integrating search and context for analysis of transfer RNA genes. *Nucleic Acids Res.* **2016**, *44*, W54–W57. [CrossRef] [PubMed]
54. Chan, P.P.; Lin, B.Y.; Mak, A.J.; Lowe, T.M. tRNAscan-SE 2.0: Improved detection and functional classification of transfer RNA genes. *Nucleic Acids Res.* **2021**, *49*, 9077–9096. [CrossRef] [PubMed]
55. Katoh, K.; Toh, H. Improved accuracy of multiple ncRNA alignment by incorporating structural information into a MAFFT-based framework. *BMC Bioinform.* **2008**, *9*, 212. [CrossRef] [PubMed]
56. Greiner, S.; Lehwark, P.; Bock, R. OrganellarGenomeDRAW (OGDRAW) version 1.3.1: Expanded toolkit for the graphical visualization of organellar genomes. *Nucleic Acids Res.* **2019**, *47*, W59–W64. [CrossRef] [PubMed]
57. Ax, P.; Armonies, W. Amphiatlantic identities in the composition of the boreal brackish water community of Plathelminthes. *Microfauna Mar.* **1987**, *3*, 7–80.
58. Noldt, U. Kalyptorhynchia (Platyhelminthes) from sublittoral coastal areas near the island of Sylt (North Sea). I. Schizorhynchia. *Microfauna Mar.* **1989**, *5*, 7–85.
59. Schilke, K. Kalyptorhynchia (Turbellaria) aus dem Eulitoral der deutschen Nordseeküste. *Helgol. Wiss. Meeresunters.* **1970**, *21*, 143–265. [CrossRef]
60. Ax, P. *Plathelminthes aus Brackgewässern der Nordhalbkugel*; Akademie der Wissenschaften und der Literatur Mainz: Mainz, Germany, 2008; Volume 1, pp. 1–696.
61. Jimi, N.; Hookabe, N.; Imura, S.; Diez, Y.L. Two new species of Schizorhynchia (Kalyptorhynchia, Rhabdocoela, Platyhelminthes) from Japan. *Zoosyst. Evol.* **2024**, *100*, 1585–1598. [CrossRef]
62. Meixner, J. Turbellaria (Strudelwürmer). In *Die Tierwelt der Nord- und Ostsee*; Grimpe, G., Wagler, E., Eds.; Akademische Verlagsgesellschaft: Leipzig, Germany, 1938; Volume 33, 146p.
63. Gobert, S.; Reygel, P.; Artois, T. Schizorhynchia (Platyhelminthes Rhabdocoela) of Lanzarote (Canary Islands), with the description of eight new species. *Mar. Biodivers.* **2019**, *49*, 2089–2107. [CrossRef]
64. Wiens, J.J. Missing data, incomplete taxa, and phylogenetic accuracy. *Syst. Biol.* **2003**, *52*, 528–538. [CrossRef] [PubMed]
65. Karling, T.G. Structural and systematic studies on Turbellaria Schizorhynchia (Platyhelminthes). *Zool. Scr.* **1983**, *12*, 77–89. [CrossRef]
66. Wey-Fabrizius, A.R.; Podsiadlowski, L.; Herlyn, H.; Hankeln, T. Platyzoan mitochondrial genomes. *Mol. Phylogenet. Evol.* **2013**, *69*, 365–375. [CrossRef] [PubMed]

67. Telford, M.J.; Herniou, E.A.; Russell, R.B.; Littlewood, D.T.J. Changes in mitochondrial genetic codes as phylogenetic characters: Two examples from the flatworms. *Proc. Natl. Acad. Sci. USA* **2000**, *97*, 11359–11364. [CrossRef] [PubMed]
68. Wolstenholme, D.R. Animal mitochondrial DNA: Structure and evolution. *Int. Rev. Cytol.* **1992**, *141*, 173–216. [CrossRef] [PubMed]
69. Bachmann, L.; Fromm, B.; Patella de Azambuja, L.; Boeger, W.A. The mitochondrial genome of the egg-laying flatworm *Aglaiogyrodactylus forficulatus* (Platyhelminthes: Monogenoidea). *Parasites Vectors* **2016**, *9*, 285. [CrossRef] [PubMed]
70. Vanhove, M.P.M.; Tessens, B.; Schoelinck, C.; Jondelius, U.; Littlewood, D.T.J.; Artois, T.; Huyse, T. Problematic barcoding in flatworms: A case-study on monogeneans and rhabdocoels (Platyhelminthes). *ZooKeys* **2013**, *365*, 355–379. [CrossRef] [PubMed]
71. Egger, B.; Bachmann, L.; Fromm, B. *Atp8* is in the ground pattern of flatworm mitochondrial genomes. *BMC Genom.* **2017**, *18*, 414. [CrossRef] [PubMed]
72. Shimada, D.; Hiruta, S.F.; Takahoshi, K.; Kajihara, H. Does *atp8* exist in the mitochondrial genome of Proseriata (Metazoa: Platyhelminthes)? *Anim. Gene* **2023**, *30*, 200161. [CrossRef]
73. Le, T.H.; Blair, D.; Agatsuma, T.; Humair, P.-F.; Campbell, N.J.H.; Iwagami, M.; Littlewood, D.T.J.; Peacock, B.; Johnston, D.A.; Bartley, J.; et al. Phylogenies inferred from mitochondrial gene orders—A cautionary tale from the parasitic flatworms. *Mol. Biol. Evol.* **2000**, *17*, 1123–1125. [CrossRef] [PubMed]

Disclaimer/Publisher's Note: The statements, opinions and data contained in all publications are solely those of the individual author(s) and contributor(s) and not of MDPI and/or the editor(s). MDPI and/or the editor(s) disclaim responsibility for any injury to people or property resulting from any ideas, methods, instructions or products referred to in the content.